DISE contributes to neurotoxicity in Alzheimer's disease

Bidur Paudel[1,10], Si-Yeon Jeong[1,10,11], Carolina Pena Martinez[2], Alexis Rickman[2], Ashley Haluck-Kangas[1], Elizabeth T. Bartom[3,4], Kristina Fredriksen[5], Amira Affaneh[5], John A. Kessler[5], Joseph R. Mazzulli[5], Andrea E. Murmann[1], Emily Rogalski[6,7], Changiz Geula[6,7], Adriana Ferreira[8], Bradlee L. Heckmann[2], Douglas R. Green[9], Katherine R. Sadleir[5], Robert Vassar[5, 6], and Marcus E. Peter[1,3,*]

Author details

[1]Department of Medicine/Division Hematology/Oncology, [3]Department of Biochemistry and Molecular Genetics, [4]Department of Preventive Medicine/Division of Biostatistics, [5]Davee Department of Neurology, [6]Mesulam Center for Cognitive Neurology and Alzheimer's Disease, [7]Department of Psychiatry and Behavioral Sciences, [8]Department of Cell and Developmental Biology, Feinberg School of Medicine, Northwestern University, Chicago, IL 60611, [2]USF Health Byrd Alzheimer's Center and Neuroscience Institute; Department of Molecular Medicine, Morsani College of Medicine, Tampa, FL 33613, [9]Department of Immunology, St. Jude Children's Research Hospital, Memphis, TN, 38105w

[11]Current address: Ministry of Food and Drug Safety, Pharmaceutical Safety Bureau, Pharmaceutical Policy Division 187, Osongsaengmyeong 2-ro, Osong-eup, Heungdeok-gu, Cheongju-si, Chungcheongbuk-do, Republic of Korea

*Correspondence: Marcus Peter, E-mail: m-peter@northwestern.edu

[10]Shared first authorship

Short title: The role of DISE in Alzheimer's disease

Abstract

Alzheimer's disease (AD) is characterized by progressive neurodegeneration, but the specific events that cause cell death remain poorly understood. Death Induced by Survival gene Elimination (DISE) is a recently discovered powerful cell death mechanism mediated by short (s) RNAs including micro (mi) RNAs acting through the RNA induced silencing complex (RISC). G-rich 6mer seed sequences in the sRNAs (position 2-7) target hundreds of C-rich seed matches in genes essential for cell survival resulting in the simultaneous activation of multiple cell death pathways. Using Argonaute precipitation and RNAseq (Ago-RP-Seq) we analyzed RISC bound sRNAs (R-sRNAs) in *in vitro* cell line models and in the brains of two *in vivo* AD mouse models and aged mice. In cell line studies we find evidence for a contribution of RNAi to the cell death and DNA damage induced by toxic Aβ42 oligomers. In addition, in AD mouse models and in the aging brain R-sRNAs RISC bound sRNAs show a shift to more toxic seeds. In contrast, in cells of "SuperAgers", individuals over age 80 who have superior memory performance, R-sRNAs are shifted to more nontoxic seeds, supporting a protective function of miRNAs. Cell death induced by Aβ42 oligomers can be rescued by adding back protective miRNAs. Our data provide first evidence of a contribution of RNAi to the neurotoxicity and DNA damage seen in AD suggesting that increasing the levels of protective miRNAs in the brain or blocking the activity of toxic R-sRNAs could lead to a novel way of treating the disease.

Keywords: DISE, tau, neurotoxicity, RNAi

Introduction

Alzheimer's disease (AD) is characterized by neurodegeneration, but the specific events that cause neuronal dysfunction and death remain poorly understood. Plaques, composed of Aβ, and accumulation of hyper-phosphorylated tau protein (p-tau) into filaments and eventually neurofibrillary tangles (NFT) are at the base of the pathology of Alzheimer's disease (AD) [1]. Neuronal loss characterizes the end stage AD pathology and multiple cell death pathways have implicated in this process [2, 3]. Toxicity by amyloid precursor protein degradation fragments such as Aβ42 is well established [4] and a strong genetic association exists between early-onset familial forms of AD (FAD) and Aβ42 [5]. More recently, it has been recognized that DNA damage accelerated by aging causes accumulation of somatic DNA alterations in individuals with AD [6, 7]. An RNA component has not been described to contribute to the etiology of AD.

RNA interference (RNAi) is a form of post-transcriptional regulation exerted by 19-25 nt long double stranded (ds) RNAs that negatively regulate gene expression at the mRNA level. The physiological way to induce RNAi is mostly mediated via miRNAs. They silence with the help of their seed at positions 2-7/8 of the miRNA guide strand [8]. The minimum seed length is 6 nucleotides [8, 9]. Matching complementary regions (seed matches) predominantly located in the 3' untranslated region (3'UTR) of mRNAs are targeted [9] resulting in cleavage-independent translational silencing [10]. miRNAs are transcribed in the nucleus as primary miRNA precursors (pri-miRNA) [11] which are first processed by the Drosha/DGCR8 microprocessor complex into pre-miRNAs [12], and then exported from the nucleus to the cytoplasm [13]. Once in the cytoplasm, Dicer/TRBP processes them further [14, 15] and these mature dsRNA duplexes are then loaded onto Argonaute (Ago) proteins to form the RNA induced silencing complex (RISC) [16]. Consequently, the deletion of either Drosha or Dicer results in the loss of almost all miRNAs [17].

We previously discovered that any RISC bound short RNA (sRNA) that carries a G-rich 6mer seed can kill cells by targeting essential survival genes in a RISC and Ago2 dependent fashion ([18, 19] and 6merdb.org). Cells die of simultaneous activation of multiple cell death pathways [20]. DISE (for Death Induced by Survival gene Elimination) [21] is an powerful evolutionary conserved cell death mechanism active in humans and rodents. We found that the ratio of miRNAs with toxic versus nontoxic seeds determines their sensitivity to DISE [22]. The most abundant miRNAs are devoid of G-rich seeds and hence not toxic to cells [18]. However, certain tumor suppressive miRNAs (e.g. miR-34a/c-5p or miR-15/16-5p) use this mechanism to kill cancer cells [18, 23]. We wondered whether diseases existed in which this anticancer mechanism was overactive resulting in reduced cancer incidence but with tissue loss due to too much cell death. We focused on AD as a candidate because patients with advanced AD have lower cancer rates and late-stage cancer patients are less likely to develop dementia [24, 25, 26].

We now demonstrate that DISE may contribute to neuronal cell death and DNA damage in AD. Our data demonstrate that exposure of differentiated SH-SY5Y (SH) cells to Aβ42 oligomers results in a shift of RISC bound sRNAs (R-sRNAs) to more toxic seeds and that cells with reduced ability to produce most miRNAs (e.g., lacking Drosha expression) are hypersensitive to sRNAs with toxic seeds and to Aβ42. In addition, inhibiting RISC function or deletion of Ago2 reduces the toxicity of Aβ42 and blocks Aβ42 induced DNA damage. Supporting the contribution of DISE to neurotoxicity seen in AD we show that in two mouse models of AD with neuronal cell death and in induced pluripotent stem cell (iPSC) derived neurons from AD patients the median seed viability of R-sRNA in brains is reduced. We provide evidence for the role of miRNAs in protecting aging brains from DISE as the aging mouse brain loses expression of protective miRNAs. In addition, R-sRNAs from brains of a group of old individuals (>80 years) with memory capacity of 50-60 year-olds (SuperAgers) have a higher seed viability than R-sRNAs in the brains of age-matched control individuals. Consequently, cells can be protected against the toxicity of Aβ42 by reintroducing protective miRNAs. In summary, we provide first evidence of a contribution of DISE to the neurotoxicity seen in AD suggesting that increasing the levels of protective miRNAs in the brain could lead to a novel way of treating the disease.

Methods

Reagents and antibodies

The following reagents and antibodies were used (sources given in brackets): Dibutyl cyclic AMP (dbcAMP) (Sigma Aldrich #D0260), *all-trans* retinoic acid (RA) (Sigma Aldrich #R2625), Brain-derived neurotrophic factor (BDNF) (GeminiBio #300-104P), Amyloid β-Protein (Aβ42) trifluoroacetate salt (Bachem #H-8146.5000), Amyloid β-Protein (Aβ40) trifluoroacetate salt (Bachem #H-1194.5000), Aurintricarboxylic Acid (ATA) (Sigma Aldrich #189400), Enoxacin (Millipore Sigma # 557305), Opti-MeM (Thermo Fisher Scientific #31985088), Lipofectamine RNAimax (Thermofisher Scientific #56532), Lipofectamine 3000 (Thermofisher Scientific #100022052), 1,1,1,3,3,3-Hexafluoro-2-Propanol (HFIP)(Sigma Aldrich #105228), Argonaute-2 Rabbit pAb (Abcam #ab32381), Tyrosine Hydroxylase Rabbit pAb (TH)(Cell Signaling #2792), GAP43 (D9C8) Rabbit mAb (Cell Signaling #8945), Tau1 Mouse mAb (Millipore Sigma #MAB3420), Drosha (D28B1) Rabbit mAb (Cell Signaling #3364), Goat Anti-Rabbit 2°Ab (Southern Biotech #4030-05), Goat Anti-Mouse 2°Ab (Southern Biotech #1070-05), HRP-conjugated β-Actin (C4) Mouse mAb (Santa Cruz Biotechnology #Sc-47778), Phospho-Histone H2A.X (Ser139) (20E3) Rabbit mAb (Cell Signaling #9718). Neuronal class III β tubulin (TUJ1) (mAb Covance #MMS-435P, 1:2000), LMX1A (pAb, Merck-Millipore #AB10533, 1:1000), Tyrosine Hydroxylase (pAb, Merck-Millipore #657012, 1:1000), HNF-3 beta (FOXA2) (mAb, Santa Cruz # sc-101060, 1:100).

Aβ peptide preparation

Solubilization, stock preparation and oligomerization of Aβ42 was performed as previously described [27, 28] with some additional modifications. Briefly, lyophilized Aβ42 was allowed to equilibrate at room temperature for 30 min and resuspended in ice cold HFIP under fume hood to obtain 1 mM solution. To disintegrate previously formed random oligomers and achieve complete monomerization, solution was vortexed vigorously for 1 min and kept at RT for 2 hrs. After monomerization, peptide solution is aliquoted in desired volumes into 1.5 ml microcentrifuge tubes, air dried overnight and then transferred to SpeedVac for another 2 hrs to remove traces of HFIP. Complete removal of HFIP and quality of monomer formation is validated by the formation of clear peptide film observed at the bottom of the tubes. Tubes containing peptide films were parafilmed and stored at -80°C for further use. For oligomerization, tube containing peptide film is dissolved in DMSO at 5 mM, vortexed for 30 sec and sonicated in the water bath for 10 min for complete suspension. Peptide is further diluted to 100 μM, vortexed, briefly centrifuged and kept at 4°C for 24 hrs for oligomer formation. Media to dilute peptide depended on the experimental condition and lacked FBS and phenol red components. After 24 hrs low molecular weight soluble peptide oligomers were retrieved by centrifugation at 14,000g for 10 min and applied at various concentrations in toxicity assays. To control for HFIP toxicity Aβ40 was prepared in the same manner as Aβ42.

Cell culture

Human neuroblastoma cell lines; SH-SY5Y (# CRL-2266™) (SH cells) were purchased from ATCC and NB7 were kindly provided by Dr. Jill Lahti (St. Jude Children's Research Hospital, Memphis, TN). SH-SY5Y cells were cultured in Dulbecco's Eagle's medium (DMEM) (Corning # 10-013-CM) and NB7 cells in RPMI 160 medium (Corning # 10-040-CM), both supplemented with 10% heat inactivated fetal bovine serum (FBS) (Sigma-Aldrich # 14009C, 1% L-glutamine (Corning # 25-005-CI) and 1% penicillin/streptomycin Corning # 30-002-CI). Cells were maintained at 37°C in saturated humidity atmosphere of 95% air and 5% CO_2. The two tau k.o. clones 232P and 231K were obtained from Dr. Paolo Paganetti (Laboratory for Biomedical Neurosciences, Ente Cantonale Ospedaliero, Torricella-Taverne, Switzerland). These cells were cultured on complete DMEM media supplemented with 1% non-essential Amino Acids (NEAA) (Cambrex Bio Science # 13-114E).

Generation of k.o. cells

NB7 Drosha k.o. cells were generated using the Alt-R CRISPR-Cas9 System (IDT DNA Technologies) following the manufacturer's protocol with the following modifications. A paired set of sgRNAs, one targeting in exon 2 (IDT predesigned gRNA Hs.Cas9.DROSHA.1.AB GUACAAAGUCUGGUCGUGGA) and one targeting downstream of exon 32 (IDT custom design AUAACUUGAUGAACAGCCAC) were annealed with the Alt-R Crispr Cas9 tracrRNA 5' ATTP 550 (#1077024) and mixed 1:1. The sRNA mix (22 pmol) was incubated with 18 pmol Alt-R Cas9 Nuclease V3 (#1081058) diluted in Resuspension Buffer R (Invitrogen #MPK10025). The Invitrogen Neon Transfection System was used to transfect the Cas9-sgRNA complex into $2x10^5$ NB7 cells in 200 mL Resuspension Buffer R with Cas9 electroporation enhancer (1200 volts, 30 ms width, 1 pulse). The next day single PE^+ cells were sorted into 96-well plates and cultured for ~ 6 weeks. SH-SY5Y Ago2 d.k.o. pool was generated by Synthego using the guide RNA sequence: UAAUUUGAUUGUUCUCCCGG. Single cells were

sorted into 96-well plates with 50% conditioned media by FACS. Knockout clones were confirmed by western blot.

Cell growth and viability assessment

Transfection of all cell lines (SH, NB7 and their Drosha k.o. clones) were performed in TPP 96 well plate (Millipore Sigma # 92696) in 250 μl final volume. Briefly, 50 μl Opt-MeM containing sRNA-lipofectamine RNAiMax (NB7) or sRNA-lipofectamine 3000 (SH) complex was forward transfected to 200 μl cells containing 3,000 NB7 cells/well or 6,000 SH cells/well. The optimized amount of lipofectamine RNAiMax or lipofectamine 3000 for both cell lines was 0.3 μl. Short (s)RNAs used to transfect these cells were sNT1, sGGCAGU, sGGGGGC or sCAG (sequences all with their guide strands modified by 2'-O-methylation of their positions 1 and 2 as previously reported [19, 29]). Following transfection, cell growth was monitored for at least 160 hrs in the IncuCyte Zoom live-cell imaging system (Essen Bioscience) with a 10X objective. The cell confluency curves were generated using IncuCyte Zoom software (version 2015A). To determine the presence of metabolically active cells after various treatments, ATP quantification was performed using Cell/Titer-Glo Luminescent Cell Viability Assay Kit (Promega # G7571). Following Aβ40/Aβ42 or ATA treatment in 96 black well plate, an equal volume of Cell Titer-Glow reagent was added to the amount of cell culture media in the well. The contents were mixed in orbital shaker for 2 min to induce cell lysis and incubated for another 10 min to stabilize the luminescent signal. Subsequently, luminescence signal was recorded using microplate reader (BioTek Cytation 5).

Differentiation of SH cells

SH cells were differentiated into neuronal-like phenotypes by two methods as described previously, one by using dbcAMP [30] and other by the combination of retinoic acid (RA) and brain-derived neurotrophic factor (BDNF) [31, 32]. Briefly, SH cells maintained in DMEM media were seeded at a density of 10,000 cells/well in 96 black well plate. After 24 hrs, DMEM media was removed, and cells were differentiated with 1 mM dbcAMP in Nb-active no phenol red (BrainBits # NbActiv4-PR) media for 7 days. At day 5 of differentiation, undifferentiated cells were again seeded at same density in parallel. At day 7, when cells were differentiated, they were treated with 20 μM (unless otherwise noted) Aβ40/Aβ42 for 48 hrs and ATP cell viability was measured as described before. To achieve neuron-like differentiation by RA/BDNF, cells were first pre-differentiated with 10 μM RA in complete DMEM media for 5 days and then treated with 50 ng/ml BDNF in the same media that lacked FBS and phenol red for additional 2 days. Seven days differentiated neuron-like cells were then used to assess toxicity of Aβ40/Aβ42 in all experiments involving differentiated SH cells.

Hydrogen peroxide treatment

NB7 and NB7 Drosha k.o. clones (A3-3, A3-11) were seeded in 96 black well plate (3,000 cells/well) in complete RPMI media. After 24 hrs cells were treated with 25 and 50 μM H_2O_2 for 3 hrs and allowed to recover for 21 hrs and ATP cell viability was measured as described above. To validate ATP data, another 96 black well plate with similar experimental design was run in an IncuCyte machine to monitor the effect of H_2O_2 on cell proliferation (data not shown).

Aurintricarboxylic acid and Enoxacin treatment

Stock solution of ATA was prepared in 0.1 M NaOH and Enoxacin in 1 M NaOH. Prior to sRNAs transfection or treatment with Aβ42 cells were pretreated with indicated concentrations of ATA for 2-24 hrs and its presence was continued throughout the analyses. In the case of Enoxacin cells were only pretreated for 24 hrs.

RNA extraction, reverse transcription, and quantitative real time PCR

Monolayer of 1.0 x 10^6 cells grown in 6 well plate was lysed in 500 µl/well QIAzol Lysis Reagent (Qiagen #79306) and RNA extraction was performed with QIAzol miRNeasy Mini Kit (Qiagen #217004) according to manufacturer's instruction. All RNA samples were subjected to DNAse digestion using RNAse-free DNAse set (Qiagen #79256) and eluted in 35 µl ultra-pure H_2O. RNA quality control was performed with Nanodrop 2000c spectrophotometer. Subsequently, 100 ng RNA was reverse transcribed using High-Capacity cDNA Reverse Transcription Kit (Applied Biosystems # 4368813) in 15 µl. cDNA was further diluted in ultra-pure H_2O to 45 µl, and qPCR was performed with TaqMan Universal PCR Master Mix (Thermo Fisher scientific #4324020) using 5 µl cDNA in a 20 µl total volume. Assay was run on 7500 Real Time PCR System (Applied Biosystems). Small nucleolar RNA (Z30) (Thermo Fisher Scientific, #001092) that have been reported to show good abundance and relatively stable expression was used as an endogenous control. Primers used to quantify expression levels of miRNAs in Parental and Drosha k.o. clones were hsa-miR-21 (Thermo Fisher Scientific, #0003970), Let-7a

(Thermo Fisher Scientific # 000377), hsa-miR-221 (Thermo Fisher Scientific #000524) and hsa-miR-182 (Thermo Fisher Scientific #002334). Relative expression of miRNAs run in triplicates were normalized to the levels of Z30 and expressed as $2^{-\Delta\Delta Ct}$.

Western blot analysis

Cell pellets containing ~1.0 x 10^6 cells were lysed in 250 µl RIPA buffer (150 mM NaCl, 10 mM Tris HCl pH 7.2, 1% SDS, 1% TritonX-100, 1% deoxycholate, 5 mM EDTA) supplemented with 1 mM PMSF and protease inhibitor cocktail (Roche #11836170001). To ensure complete lysis, cells were kept on ice for 30 min, vortexed occasionally and sonicated. Lysed cells were then boiled for 10 min at 95°C and centrifuged (14,000 rpm at 4°C) for 15 min. Protein quantification was performed with DC Protein Assay Reagent (BIO RAD) in an iMark Microplate Reader (BIO RAD) at 750 nm. 20 µg protein per lane was run on SDS-polyacrylamide gel electrophoresis (SDS-PAGE) (BIO-RAD #1610158) at 40 mA for ~1 h. Resolved proteins were then transferred to Nitrocellulose Blotting Membrane (Healthcare #10600016) at 250 mA for 2 hrs on ice. Transferred membranes were then blocked with 5% non-fat dry milk for 1 hr at room temperature in TBST (Tris-buffered saline, 0.1% Tween 20) and immunoblotted with various antibodies overnight (1:1000 in 3% BSA in TBST). Following primary antibody incubation, membranes were washed with TBST and probed with secondary Goat-anti-Rabbit or Mouse IgG HRP (1:5000 in 1% milk for 1 hr at RT). Finally, membranes were washed and developed with Super Signal West Dura Luminol/Enhancer (Thermo Scientific #1859025).

Western blot analysis of iPSC derived midbrain dopamine neurons: Cultures were harvested at different time points as indicated in the figures and lysed in 1% Triton X-100 buffer containing protease inhibitor cocktail (Roche diagnostics, # 11-836-170-001), 1 mM PMSF, 50 mM NaF, 2 mM sodium orthovanadate by homogenization and incubation on ice for 30 minutes. The protein concentration was determined by using micro-BCA kit (ThermoFisher, # 23235) and 40 µg of lysates were loaded onto 10% Tris/glycine PAGE gels followed by transfer onto PVDF membranes (EMD Millipore, # IPFL00010) at 30V for 1hr). Membranes were post-fixed in 0.4% paraformaldehyde, washed in milliQ water and then blocked in 1:1 TBS : odyssey blocking buffer (Licor # P/N 927-40003) for 1 hr at room temperature. The membrane was incubated with primary antibodies diluted in 1:1 ratio 0.2% TBS-tween and odyssey blocking buffer overnight at 4°C. The following day the membrane was washed with 0.2% TBS-Tween and incubated with secondary antibodies for 1 hr. Anti-rabbit IgG conjugated to IRDye800 and anti-mouse IgG conjugated to Alexa 680 were used for simultaneous detection of both channels on the same blot. The blot was washed as before and scanned on an odyssey imaging system. The western blots were analyzed using Image Studio software (Licor) to quantify band intensities.

Mouse brain tissue

All animal experiments were approved and conducted in accordance with IACUC regulations at Northwestern University, St. Jude's Children's Hospital and University of South Florida, Tampa. 5XFAD mice were bred in house by crossing 5XFAD transgenic males (line 6799) to B6/SJL F1 hybrid females and genotyped as described [33]. Mice were sacrificed by CO_2 inhalation. One hemibrain was snap-frozen in liquid nitrogen. Three transgenic and three non-transgenic females were used for analysis. 6- or 8-month-old female 5XFAD Rubicon$^{+/-}$ or 5XFAD Rubicon$^{-/-}$ mice [34]; or 3-month-old male control and human tau45-230 transgenic mice generated using the human cDNA coding sequence for tau45-230 under the control of the Thy 1.2 promoter on a C57BL/6J background [35].

Written informed consents were obtained from all human participants and the study was approved by the Northwestern University Institutional Review Board and in accordance with the Helsinki Declaration. Frozen brain tissue from the middle frontal gurus of 5 cognitively normal elderly participants, 7 clinically and pathologically confirmed AD patients [36, 37] and three cognitive SuperAgers were obtained from the Northwestern University Alzheimer's Disease Center Brain Bank. Brains of cognitively normal individuals were free of neurodegenerative pathology, except for age-appropriate accumulation of plaques and tangles [37]. SuperAgers participants were enrolled in the Northwestern University SuperAging Program, were 80 years or older, were required to perform on the Reys Auditory Verbal Learning test of episodic memory equal to or better than individuals 20-30 years younger, and on tests of other cognitive domains equal to or better than same-age peers [38] Age at death and postmortem interval were not different among the three groups ($p>0.05$). Please see Supplementary Table 1 for characteristics of participants.

Written informed consents were obtained from all human participants and the study was approved by the Northwestern University Institutional Review Board and in accordance with the Helsinki Declaration. Frozen brain tissue from the middle frontal gurus of three cognitively normal elderly participants and three cognitive SuperAgers were obtained from the Northwestern University Alzheimer's Disease Center Brain Bank. Brains of cognitively normal individuals were free of neurodegenerative pathology, except for age-appropriate

accumulation of plaques and tangles [37]. SuperAgers participants were enrolled in the Northwestern University SuperAging Program, were 80 years or older, were required to perform on the Reys Auditory Verbal Learning test of episodic memory equal to or better than individuals 20-30 years younger, and on tests of other cognitive domains equal to or better than same-age peers [38]. Age at death and postmortem interval were not different among the two groups ($p>0.05$). Please see Supplementary Table 1 for characteristics of participants.

TUNEL staining of mouse brains

Brains of the indicated genotypes were harvested from mice following transcardic perfusion with 4% PFA in PBS. Harvested brains were immediately placed in 4% PFA and fixed overnight at 4°C. Brains were then briefly washed with cold PBS and transferred to 30% sucrose for cryoprotection. Brains were oriented following sagittal segmentation in OCT, sectioned, and mounted on glass slides. TUNEL staining was performed using the 594-TUNEL Assay Kit (Cell Signaling #48513) per the manufacturer's instructions. In brief, slides were rinsed in PBS to remove residual OCT medium and then permeabilized in 5% BSA/0.2% TX-100 in PBS for 30 min. Slides were washed two times in PBS then incubated for 5 min in TUNEL equilibration buffer. Next, slides were incubated for 2 hrs at 37C in TUNEL reaction mix in a humidified, dark environment. Slides were then washed 3 times in BSA/TX PBS solution above. Finally, coverslips were applied using Prolong Diamond Antifade Mountant with DAPI (Invitrogen P36931).

Slides were then imaged on a Nikon Ti-E epifluorescence microscope with Andor Clara ECCD camera and processed using Nikon Advanced Research (NIS) Elements software. Quantification of TUNEL+ cells was achieved by automatically defining and separately masking TUNEL signal and the DAPI signal using NIS Elements. TUNEL+ cells were defined where TUNEL signal was observed in the DAPI masked area using automated analysis. Automated results were subsequently verified by manual counting. TUNEL signal that was observed outside of the DAPI masked area was not included in this analysis for both automated and manual counting, although may represent additional cell death in cells that no longer stain DAPI positive.

iPSC derived excitatory forebrain neurons from AD patients

Generation of iPSC lines from AD patients (AD1: AG5810-F [APOE3/4]; AD2: AG011414 [APOE3/4]) and healthy controls (Control 1 NUAD0635 [PBMC], Control 2: AG02261 [APOE3]) were previously described and obtained from Coriell Institute for Medical Research [39] (AG5810, AG011414, AG002261) or provided by Northwestern University's Mesulam Center for Cognitive Neurology and Alzheimer's Disease (NUAD0635). iPSCs were differentiated to forebrain excitatory neurons via lentiviral-mediated overexpression of *neurogenin-2*, as previously described [40] with minor modifications. Stem cells were maintained in mTeSR1 media (Stemcell Technologies) on Matrigel coated dishes (Corning). Upon start of differentiation, cells were single cell dissociated using Accutase (Millipore) and resuspended in mTeSR1 with 10 μM ROCK Inhibitor Y-27632 with lentiviruses encoding rrTA and pTetO-Ngn2-puro (generated by the Northwestern University Skin Biology & Diseases Resource-Based Center. The following day, medium was changed to KO-DMEM (Thermo Fisher Scientific), 1X MEM nonessential amino acids, 1X Glutamax, and 0.1% 2-mercaptoethonal, supplemented with 10 μM SB431542 (Stemgent), 100 nM LDN193189 (Stemgent), 2 μM XAV939 (Tocris Bioscience, Bristol, UK), and 3 μg/ml doxycycline (Sigma). Gradually, medium was changed over 2 days to neural induction medium, DMEM/F-12 containing MEM nonessential amino acids, Glutamax, N-2 (Thermo Fisher Scientific), D-glucose (Sigma), 2 μg/ml heparin sulfate (Sigma) supplemented with 3 μg/ml doxycycline and 2 μg/ml puromycin. Induced neurons were replated onto 6-well tissue culture plates at 450k cells/well on pre-coated with poly-L-orthnithine (Sigma), 4 μg/ml Laminin (Roche Basel, Switzerland), and 2 μg/ml Fibronectin (Sigma), cultured with neuronal maturation medium (BrainPhys Basal Medium [Stemcell Technologies], B-27 and N-2 supplements [Thermo Fisher Scientific], MEM nonessential amino acids, and Glutamax, supplemented with 3 μg/ml doxycycline and 10 ng/ml BDNF [R&D systems]). Post-plating, cells were treated with 3 μM Ara-C for 48 hrs to eliminate proliferating cells. Half of the medium was exchanged every 2 to 3 days until cell collection.

iPSC derived midbrain dopamine neurons used for *in vitro* aging study

Human iPSC from a previously characterized healthy control (line 2135 or C3 in [41]) were cultured in mTeSR1 media (Stemcell Technologies) on vitronectin coated dishes. iPSCs were dissociated into single cells by accutase treatment and seeded at 5,000 cells per cm^2 in a Matrigel coated dish. Differentiation was carried out as described [41] using dual SMAD inhibition followed by stimulation of sonic hedgehog and canonical WNT signaling. Cells were passaged en bloc at day 15 and then manually passed onto 10 cm dishes coated with poly-D-lysine at 66 μg/ml (Sigma # P1149) and laminin at 5 μg/ml (Roche # 11243217001). Cells were cultured in the presence of differentiation factors for 40 days, and then maintained in Neuraobasal media (Life Technologies)

supplemented with Neurocult SM1 (Stemcell Technologies) and 1% penicillin / streptomycin (Life Technologies) until harvesting up to day 190.

To characterize iPSC derived neurons by immunocytochemistry, differentiated midbrain neurons were fixed in 4% paraformaldehyde in phosphate buffered saline (Life Technologies) for 20 min followed and permeabilized / blocked in PBS with 0.3% Triton X-100 containing 2% bovine serum albumin and 3% normal goat serum for 30 min. Primary antibodies were added and incubated overnight at 4°C in blocking buffer. Cells were then incubated in anti-mouse or rabbit IgG conjugated Alexa 488 (1:400) or Alexa 568 (1:200) (Life Technologies) for 1 hr, washed, then mounted in 10 μl of 4,6-diamidino-2-phenylindole dihydrochloride (DAPI)-containing Fluoromount G (Southern Biotech, #0100-20). Coverslips were analyzed by microscopy using a Leica confocal microscope (Leica TCS SPE laser at 25-50% power; CTR4000 / DMI4000B microscope) through a 10 μm section (z-series at 1 μm per section). The percentage of each cell population (FOXA2 / TH; LMX1A / βiiiTubulin) was quantified and normalized to total cell number through DAPI staining.

Ago pull-down and subsequent small RNA-seq (Ago-RP-Seq)

Ago pull down of the samples used in the study was performed as previously described [22]. Briefly, frozen brain pieces mouse (~150 mg, cortex and hippocampus combined) and the cell pellets obtained from iPSC derived neurons (10^6), RA/BDNF differentiated SH cells (1.5 x 10^6), NB7 parental and Drosha k.o. clones (10^6), NB7 cells transfected with sRNAs (1.5x10^6) were lysed in 1 ml NP40 lysis buffer [50 mM Tris pH 7.5, 150 mM NaCl, 5 mM EDTA, 0.5% NP-40, 10% (v/v) glycerol, 1 mM NaF; supplemented with 1:200 EDTA-free protease inhibitors (Millipore #539134) and 1:1000 RNaisin Plus (Promega #N2615) before use]. For complete lysis, cells were kept on ice for 15 min, vortexed occasionally, and then centrifuged at 20,000g for 20 min. In the case of brain tissue samples, lysates were prepared by homogenizing tissues several times using Dounce Tissue Grinder in the same lysis buffer (Duran Wheaton Kimble # 357538). Pull down of Ago proteins (Ago 1-4) was performed by incubating 500 µg of Flag-GST-T6B peptide [42] (Sigma #M8823) with 80 µl of anti-Flag M2 Magnetic beads (Sigma #M8823) at 4°C for 3 hrs in a rotor. Subsequently, beads were washed three times and resuspended in 1 ml NP40 lysis buffer. To confirm pull down of Ago proteins, 50 µl aliquot containing beads were mixed with 2x SDS-PAGE sample buffer and run on 10% SDS-PAGE gel for western blot analysis by anti-Ago2 antibody. After validation, remainder of the beads was used for RNA extraction using Trizol reagent (Ambion #15596018). Subsequently RNA pellet was resuspended in 20 µl ultra-pure H_2O and 10 µl was kept for RNA visualization purposes while another 10 µl was used for small RNA library preparation using Illumina primers (RRID:SCR_010233) as described previously [43]. Briefly, RNA was ligated with 3′-adenylated adapters using T4 RNA Ligase 2 (NEB #MO351) for 4 hrs at 16°C. Product was ethanol precipitated and run on 15% Urea-PAGE gel. To determine correct position of the ligated product in the gel, radiolabeled (^{32}P) unligated and ligated size markers (19-35nt) were also run in parallel. Ligated product was then eluted from the gel and prepared for 5' adaptor ligation. Ligation of 5' adaptor to already 3' ligated RNA product was performed with T4 RNA ligase 1 (NEB, #EL0021) at 37°C for 1 h. The product was again run on 12% Urea-PAGE gel, extracted and reverse transcribed using Superscript III reverse transcriptase (Invitrogen #18080–044). Enrichment of product was performed by amplifying cDNA with multiple rounds of few cycles PCR. Quality of cDNA was validated by bioanalyzer analysis with a single peak at ~157 bp length. Sequencing of cDNA was performed on Illumina Hi-Seq 4000. The sequence information on size markers, 3' and 5' adaptors, RT primers, and PCR primers were previously published [44].

6mer seed viability (SPOROS) analysis

The SPOROS pipeline [45] was used to generate seed viability graphs, seed viability plots and seed nucleotide composition analyses. Briefly small RNAseq data sets in the form of raw fastq files were de-multiplexed, trimmed, cleaned and then compiled into a single read count table. After removing rare reads as described [45], the remaining reads were BLASTed against lists of small RNAs from either mouse or human. Reads that matched artificial sequences in the database were removed and final raw read count table (rawCounts) was generated. The raw read count table was used to generate two read count tables; one normalized read count table (normCounts) that contained 1 million reads per sample, and the other normalized and differentially expressed read count table (differential). After annotating each count table with 6mer seed, average 6mer seed viability, miRNA, and RNA world data, various seed viability analyses were done. Seed viability graphs were generated by adding and collapsing all rows that contained same 6mer seed and RNA type and aggregating all the read counts within that 6mer seed viability in 1% bin size. Graphs were prepared in Excel with smoothing line function on. Shown in the graphs are the peaks of normCounts plotted against % 6mer seed viability. When determining the average seed viability or seed composition analysis each row counts were first normalized by 1000 to ease

computational complexity and the columns containing 6mer seeds and average 6mer seed viability were expanded based on the normalized read counts. Table containing frequency distribution of average 6mer viability for various groups were then used to generate basic boxplot (StatPlus (v.7.5)). Statistical analysis was done with Kruskal-Wallis test when comparing groups. Weblogo plots were generated to show average seed composition in positions 1-6. The differential expression analysis between two groups was done by taking significantly (p-value <0.05) expressed reads for each row between two groups and expressing them in delta read counts (perturbed sample-control sample). The frequency of average 6mer seed viability or 6mer seeds were then expanded based on the delta read counts to get the seed viability graph, seed viability plots, or 6 seed compositions as described above.

Availability of data and materials

RNA seq data were deposited at GEO under accession number GSE213138 (https://www.ncbi.nlm.nih.gov/geo/query/acc.cgi?acc=GSE213138). All other data generated and analyzed during this study are included in this published article and its supplementary information files.

Statistical analyses

Student's T-tests were performed in Microsoft Excel. Two-way analyses of variance were evaluated using STATA version 14.0. STATA was also used for comparing differences in polynomial distributions as described previously [18]. All other statistical analyses were conducted in R version 4.0.0.

Results

Toxic Aβ42-oligomers shift the balance of RISC-bound short RNAs to lower seed viability.

Throughout the manuscript we will be using two terms: seed viability and DISE. Seed viability refers to the viability of three human and three murine cell lines after transfection with one of 4096 6mer seeds embedded in a neutral siRNA-like backbone that carries a 2'-O-methylation at positions 1 and 2 of the passenger strand to avoid RISC uptake [18, 19]. The seed viabilities used are either based on the average % viability of the three human cells (for the analysis of human cells) or the average % viability of the three murine cells (for the analysis of mouse cells/tissue), respectively. DISE refers to the mechanism of how the toxic 6mer seed containing sRNAs kill cells. The lower the average seed viability of an sRNA, the more potent it will kill through DISE.

To determine whether DISE could be involved in the death of brain derived cells, we chose the well characterized SH-SY5Y (SH) cell line differentiated into neurons to model neurotoxicity upon treatment with Aβ42 oligomers [46, 47, 48]. Similar to other brain-derived cell lines [19], SH cells were susceptible to sRNAs that carry toxic 6mer seeds such as an sRNAs carrying the 6mer seed of miR-34a-5p (GGCAGU) [18] or the consensus toxic 6mer seed GGGGGC [19] (**Supplementary Fig. 1a**). While moderately sensitive, SH cells gain sensitivity to toxic Aβ42 oligomers after differentiation [49]. We demonstrated that our preparation of Aβ42 oligomers was soluble without aggregates (not shown) and was more active than control Aβ40 in SH cells fully differentiated for 7 days either by treating them with 1 mM dbcAMP [50] (**Supplementary Fig. 1b, c**) or by using a differentiation protocol involving retinoic acid (RA) and brain-derived neurotrophic factor (BDNF) [51] (**Fig. 1a-c**). After establishing the specific activity of Aβ42 oligomers, we decided to use the more physiologically relevant protocol of differentiating SH cells with RA and BDNF for all subsequent experiments.

We recently reported that a minor shift in the loading of toxic sRNAs into the RISC can cause activation of DISE, and that the balance of RISC-bound sRNAs with toxic versus nontoxic seeds (mostly miRNAs) can determine cell fate [22] (**Fig. 1d**). To determine whether the toxicity of Aβ42 to SH cells was associated with a shift to fewer nontoxic/protective RISC bound reads, we treated 7-day differentiated SH cells with Aβ42 for 2, 4, and 6 hours. We chose these time points to capture changes before the initiation of cell death, which was first detectable 24 hrs after treatment (**Fig. 1c**). R-sRNA were identified by an Ago1-4 peptide pulldown, and RNA precipitation combined with high-throughput sequencing (Ago-RP-Seq) as described [22]. To analyze the role of DISE in disease situations we recently developed SPOROS, a semi-automated bioinformatics pipeline to analyze seed viability of sRNAs in a gene agnostic fashion [45]. Employing the SPOROS pipeline we found that the sRNAs that were significantly enriched in the RISC of cells treated with Aβ42 compared to cells treated with Aβ40 had a significantly lower seed viability than sRNAs that were depleted in the RISC (**Fig. 1e**).

Reduced seed viability of R-sRNAs in the brains of AD mouse models with signs of neurotoxicity

The DISE mechanism is conserved between human and mouse [18, 52]. To determine if DISE contributes to neurodegeneration seen in AD, we used two established mouse models replicating the primary hallmarks of AD pathogenesis, amyloid deposition and tau pathology. The first model is based on the widely used 5XFAD mice, which develop cerebral amyloid plaques and gliosis at two months of age, achieve high Aβ42 burden, and have reduced synaptic markers and a late neuron loss. However, 5XFAD mice do not form NFTs, do not show much of an increase in staining for p-tau [33, 53], and, most relevant to this study, they do not show a significant degree of neuronal cell death up to 8 months of age [33]. Rubicon is a gene that constrains canonical autophagy [54]. In the absence of Rubicon 5XFAD mice developed accelerated disease pathology and neurodegeneration, reactive microgliosis, tau pathology, and behavioral impairment similar to what is seen in human AD patients. The most significant difference between 5XFAD and these Rubicon k.o. mice, however, was that they develop neuronal cell death early in the disease progression [34] (**Fig. 2a, b**).

The SPOROS bioinformatics pipeline which allows to visualize changes in total and R-sRNAs produces a number of graphical outputs [45]. Among them are: 1) A seed viability graph that plots sRNAs according to their abundance (Y axis) and seed viability (X axis), based on the average seed viability on three human cell lines (see 6merdb.org) and 2) The median seed viability of all sRNAs in form of a box plot. Performing an Ago-RP-Seq-SPOROS analysis we compared the content of the RISC in mouse brains (cortex and hippocampus) of 6-month-old 5XFAD Rubicon$^{-/-}$ mice with advanced disease to the brains of three symptom-free age-matched 5XFAD Rubicon$^{+/-}$ mice. A number of miRNAs which constituted >96% of the R-sRNAs were significantly differentially expressed, most notably miR-9-5p (**Fig. 2c**). Interestingly, the median seed viability in the 5XFAD Rubicon$^{-/-}$ mice was significantly reduced (**Fig. 2c**). This correlates with the increased Aβ42 levels in this model [34] and the resulting occurrence of cell death (**Fig. 2a, b**). This effect was not seen in the 5XFAD mice (data not shown).

The second model we used represents a tauopathy. It has been shown that Aβ toxicity is dependent on the presence of tau [55, 56] and tau depletion ameliorated Aβ-induced behavioral deficits when compared to transgenic mice overexpressing FAD-mutant amyloid precursor protein [55]. A growing body of evidence suggests that Aβ induces a series of post-translational tau modifications including its cleavage into a neurotoxic tau_{45-230} fragment. High levels of this fragment were detected in human brains obtained from AD and other tauopathy subjects [57]. Human and murine tau are quite different and murine tau does not form NFTs [58]. However, transgenic mice expressing human tau_{45-230} under the control of the Thy 1.2 promoter showed enhanced cell death of pyramidal hippocampal neurons as early as 3 months after birth, progressive synaptic loss in the hippocampus, and behavioral deficits when compared to wild type controls [35]. Similar to the amyloid field, it is now believed that smaller tau aggregates are more toxic than the bigger aggregates (i.e. NFT). The tau fragment expressed in the tau_{45-230} tg mice was shown to aggregate into dimers and small oligomers that are highly toxic and present in AD patient brains [59]. Furthermore, it was shown that in the presence of this fragment full-length tau forms smaller and potentially more toxic aggregates. We therefore subjected brains (hippocampi) from 3 months tau_{45-230} transgenic mice to the same analysis as the other mouse model (**Fig. 2d**). Consistent with the increase in cell death seen in this model, the median seed viability of R-sRNAs enriched or depleted in the brains of these mice was reduced by more than 10% (insert in **Fig. 2d**). Like in the previous AD model miR-9-5p was again strongly enriched in the RISC in the brain of these mice compared to control mice corroborating previous findings on the role of miR-9-5p in neurodegeneration [60, 61]. A comparison of the data from both mouse models suggested that the Ago-RP-Seq method reproducibly pulls down the same miRNAs from mouse brains. In fact, a majority of RISC bound miRNAs was found to be deregulated in both mouse models (shared miRNAs labeled in black in **Supplementary Fig. 2a,c**). The results obtained from the female 5XFAD Rubicon k.o. and the male tau_{45-230} transgenic mice available to us were quite similar suggesting no major difference between male and female mice.

We do not believe that the observed difference between normal and AD brains is due to an increase in infiltrating immune cells because an analysis of neuron, glia and macrophage/lymphocyte specific miRNAs [62, 63, 64, 65] bound to the RISC did not support that interpretation (**Supplementary Fig. 3**). In summary, the analysis of the R-sRNAs from the brains of two mouse models of dementia with signs of neuronal cell death suggest a possible contribution of DISE to the neurotoxicity seen in these models.

Reduced seed viability of R-sRNAs in AD derived iPSC neurons.

The data on the AD mouse models and the *in vitro* data on SH cells suggested that a lower seed viability is associated with an increase in neurotoxicity. To determine whether this could also be found in human neurons, we analyzed iPSC derived neurons generated from two control and two AD patients (**Fig. 3a**, **b**). AD derived iPSC neurons had highly upregulated Tau1 protein and showed signs of ongoing DNA damage stress with increased H2AX phosphorylation (**Fig. 3c**). In the AD derived cells when assessing the total R-sRNA changes a number of miRNAs with nontoxic seeds were downregulated compared to control cells (**Fig. 3d**) resulting in a drop in mean seed viability in the sRNAs that were enriched in the AD samples (**Fig. 3e**) suggesting that in cells from AD patients protective R-sRNAs may be reduced.

6mer seed viability of R-sRNAs drops during aging.

miRNAs have been shown to protect neurons from cell death [66, 67], but aging neurons may be less able to generate miRNAs [68]. Such aging neurons could be more susceptible to small RNAi active RNAs that induce cell death. To test whether aging neurons would lose their protection by nontoxic miRNAs, we compared the RISC content of the brain cells of young (2-month-old) with that of old (18-month-old) mice (**Fig. 4a**). We found that the RISC in brain cells (cortex and hippocampus) of older mice contained significantly less sRNAs with high seed viability suggesting that they may be less able to protect themself against the activity of toxic sRNAs. This was independently confirmed in an analysis of another set of young and old mice (**Supplementary Fig. 4a-e**). The miRNAs that were pulled down in these two experiments were very similar (shared miRNAs labeled in black in **Supplementary Fig. 4a, b**), median seed viabilities and seed composition of all R-sRNAs in these samples were indistinguishable (**Supplementary Fig. 4c, d**), and a Pearson correlation demonstrated high reproducibility between the two experiments (**Supplementary Fig. 4e**). Just as in experiment #1 in experiment #2 the median seed viability of the differentially expressed R-sRNA was lower in the brains of old versus young mice (**Supplementary Fig. 4f**).

How could aging neurons lose their protection by nontoxic miRNAs? A progressive loss of Dicer and the resultant global decrease in miRNA expression with age has been suggested as one mechanism. A study showed that Dicer expression in the brains of two year old mice is substantially reduced compared to the brains

of 6-week-old mice [68]. We therefore wondered whether neurons with increasing age would lose expression of some of their protective miRNAs and whether sRNAs that are enriched in older neurons could be more toxic, rendering the neurons primed for DISE. We used two approaches to address the question of whether cells with age would lose protective miRNAs:

1) We tested whether the loss of protective R-sRNAs can be seen in aged neurons *in vitro.* iPSC derived neurons were aged in a dish as described [69] (**Supplementary Fig. 5**). These cells were cultured for up to 190 days in poly-d-lysine and laminin coated dishes. We detected a substantial loss of Dicer protein with increasing age (right insert in **Fig. 4b**). An Ago-RP-Seq-SPOROS experiment suggested a small but significant decrease in seed viability in the 5-month-old versus 1-month-old iPSC derived neurons (left insert in **Fig. 4b**). While the difference seems small, we would like to point out that the analysis of total amounts of R-sRNAs, not the differentially expressed ones, is shown.

2) We analyzed a data set of a study that had reported major changes in the miRNA content of peripheral blood mononuclear cells (PBMCs) between young and old cohorts [70] because it was shown before that besides the brain spleen/immune cells is another tissue whose miRNA content changes with age [68]. A reanalysis of these data for the seed viability of the differentially expressed mature miRNAs revealed a substantial drop in median seed viability and a concomitant increase in G content of the 6mer seeds in the miRNAs upregulated in the PBMCs from the old cohort (**Fig. 4c**). This is line with our data on the mouse brains and suggests that with age certain tissues may be more primed to undergo DISE.

If the assumption is correct that a higher seed viability of R-sRNAs in brain cells protects from neuronal death and dementia and this is reduced with increasing age, then individuals that are known to be less prone to AD or other forms of dementia may maintain a higher level of protective miRNAs in the RISC similar to younger individuals. To test this hypothesis, we analyzed the RISC content of brain cells from SuperAgers which are individuals age 80 and above whose episodic memory performance is at least at the level of cognitively average individuals in their 50s and 60s [38]. We obtained post mortem brain tissue from three SuperAgers and compared them to three cognitive normal individuals of a similar age (**Supplementary Table 1**). We did indeed find that the RISC in the SuperAger brains (average age = 90 years) contained sRNAs with a significantly higher seed viability than in control brains (average age 85.7 years) (**Fig. 4d**). These preliminary data suggest that SuperAgers may have a greater resilience to the damage by toxic sRNAs which may contribute to dementia such as AD. In summary, our data are consistent with DISE contributing to the etiology of AD. Aging neurons may be more prone to this form of cell death but individuals that can maintain higher seed viability of their R-sRNAs are more resilient to AD.

Modulating RISC content alters cells sensitivity to Aβ42 induced toxicity.

We previously reported that global downregulation of most abundant miRNAs, which mainly carry nontoxic seeds, caused by deleting either Dicer or Drosha sensitizes cells to effects of toxic sRNAs [18, 21, 29, 71, 72]. To determine whether neuron derived cells gain sensitivity to Aβ42 induced cell death after removal of most miRNAs, we generated Drosha k.o. clones of the neuroblastoma cell line NB7 (**Fig. 5a**). This resulted in about 50% reduction of RISC bound miRNAs (**Fig. 5b**) with major miRNAs substantially reduced (**Fig. 5c**). Previously, we characterized Drosha k.o. HCT116 cells and reported that in the absence of protective miRNA expression most R-sRNAs were not miRNAs. With Ago2 expression levels were unaffected in these cells, the median seed viability across all R-sRNAs was much lower than that of R-sRNAs in wt cells [71].

Thus, to investigate the effect of lack of Drosha on the brain derived cells, we sequenced the total cellular sRNAs from the parental cells and two Drosha k.o. clones and analyzed the sequencing data with SPOROS. Similar to the data obtained with Drosha k.o. HCT116 cells, in the two NB7 k.o. clones, many canonical miRNAs were reduced in the total RNA and other sRNAs (i.e., rRNA and tRNA fragments) were quite prominent (**Supplementary Fig. 6a**). This resulted in a significant drop in median seed viability in both k.o. clones (**Supplementary Fig. 6b**) caused by the loss of protective miRNAs that carry nontoxic seeds. Consistent with previous data, we found that the two k.o. clones were much more sensitive to DISE induced by sGGCAGU transfection (**Supplementary Fig. 6c**).

After establishing that NB7 cells with reduced Drosha expression were hypersensitive to DISE, we tested whether the two k.o. clones were also more susceptible to cell death induced by Aβ42 than the parental cells. Parental NB7 cells were moderately sensitive to Aβ42 relative to Aβ40 (**Fig. 5d**). In contrast, both Drosha k.o. clones were ~10% more sensitive to Aβ42-induced cell death consistent with the hypothesis that miRNAs with nontoxic seeds could protect cells from this toxicity.

Having provided evidence of a contribution of DISE to Aβ42 induced cell death and miRNAs being protective, we wondered whether we could protect NB7 k.o. cells by reconstituting them with some of the nontoxic miRNAs

most downregulated in these cells. To identify such miRNAs, we performed a SPOROS analysis of R-sRNAs in wt and Drosha k.o. cells (**Fig. 5e**). While a few miRNAs with toxic seeds were increased in these cells (i.e., miR-15/16-5p), there were a larger number of miRNAs with nontoxic seeds that were strongly reduced in the two k.o. clones resulting in a clear drop in seed viability and in a more C-rich average 6mer seed in the R-sRNA of the k.o. clones (**Fig. 5f, g**). The three most highly downregulated and nontoxic miRNAs miR-21-5p, miR-25-3p, and miR-92a-3p were also the top three most abundant ones in the RISC of wt cells (**Fig. 5h**). We therefore decided to reconstitute the k.o. cells with these three miRNAs to test whether adding them back to the RISC would render cells more resistant to the toxicity exerted by Aβ42.

To test this, we transfected NB7 Drosha k.o. cells with the three miRNAs individually or with a cocktail of all three. Because any nontoxic control sRNA could be incorporated into the RISC and block its activity, we compared this with cells treated with only lipid or transfected with a control sRNA modified on both strands at position 1 and 2 with 2'-O-methylation (sNT) which we previously showed to completely prevent RISC loading (5, 29). In this experiment we found that introducing the three miRNAs individually or as a cocktail rendered cells ~10% less sensitive to Aβ42 (**Fig. 5i**). The fact that all three miRNAs protected cells from Aβ42 induced cell death to a similar degree is consistent with a model that it is not the activity of each individual miRNA and the targeting of its targets alone that determines cell fate but rather the fact that they carry nontoxic seeds and are blocking RISC access.

Aβ42 oligomers are toxic to cells in part through RNAi.

Our data suggest an association between neurotoxicity seen in AD and the seed viability of R-sRNAs. We were wondering whether mechanistically the main mediator of neurotoxicity in AD, Aβ42, kills cells with the help of the RISC and RNAi. We therefore tested the involvement of Ago2 in the toxicity elicited by Aβ42. We first used the Ago2 inhibitor aurintricarboxylic acid (ATA) [73] to determine whether toxic RNAs that kill through Ago2 showed reduced activity on RISC inhibited neuron derived cells. We treated NB7 cells with a low concentrations of ATA and showed that this inhibited DISE induced by either the two toxic seed-containing sRNAs used above or by the highly toxic Huntington's disease (HD) derived CAG trinucleotide repeat containing sRNA sCAG we recently described [29, 74] (**Supplementary Fig. 7a**). ATA inhibited toxicity induced by all three sRNAs in a dose dependent manner. Undifferentiated SH cells (used because their growth could be monitored by an IncuCyte analysis) were also protected from sCAG induced cell death by ATA (**Supplementary Fig. 7b**) and a rescue of sCAG induced cell death was observed in these cells (**Supplementary Fig. 7c**).

To determine whether ATA which at higher concentrations inhibits multiple endonucleases [75] did indeed act by inhibiting Ago2 and hence RNAi, we performed an Ago-RP-Seq analysis of NB7 cells transfected with either 1 nM sNT1, sGGGGGC or sGGGGGC in the presence of a low concentration of 10 μM ATA (**Supplementary Fig. 7d**). ATA treatment substantially prevented RISC uptake of sGGGGGC. This analysis confirmed the activity of ATA on Ago2 and suggested that the inhibition of the RISC uptake of the toxic sRNA is what protects the cells from transfection with sGGGGGC.

After establishing that ATA could protect cells from DISE induced by a toxic sRNA, we tested whether ATA which was previously shown to protect primary neurons from Aβ42 induced death [76] had an effect on Aβ42 induced cell death in differentiated SH cells at 10 μM (**Fig. 6a**). A significant 10% reduction in cell death was observed. To exclude that the effects seen with ATA were due to inhibition of nucleases other than Ago2, we deleted Ago2 in SH cells. Three clones with very low or undetectable Ago2 expression were isolated (**Fig. 6b**). Ago2 deficient cells were substantially resistant to the toxicity of transfected sCAG (**Supplementary Fig. 8**). Knock-out of Ago2 did not affect the ability of the cells to differentiate as shown by the induction of the synaptic marker GAP43 (**Fig. 6c**). However, we used undifferentiated cells for the following experiments involving these k.o. cells to prevent any effect of reduced differentiation due to impaired RISC/miRNA activity. Similar to the effects seen upon ATA treatment all three Ago2 k.o. clones were less sensitive to Aβ42 induced toxicity than the parental cells (**Fig. 6d**). Neither ATA treatment nor deletion of Ago2 completely blocked Aβ42 induced toxicity. This could be due to RISC independent pathways being activated by Aβ42 or an involvement of the other three Ago proteins expressed in human cells mediating the effects of the toxic sRNAs induced by Aβ42.

Aβ42 oligomer induced DNA damage is dependent on tau and an active RISC.

Enoxacin is an antibiotic that causes an upregulation of miRNAs by stabilizing Dicer/TRBP [77, 78] and treatment with Enoxacin has been shown to improve survival of cultured dopaminergic neurons [79]. We were therefore wondering whether Enoxacin could protect cells from the toxicity of Aβ42. To test this we pretreated differentiated SH cells with Enoxacin and exposed the cells to Aβ40/42 (**Fig. 6e**). Surprisingly, Enoxacin had little effect on cell viability but it completely blocked DNA damage induced by Aβ42 at a concentrations of 20 μM or higher. This

finding is consistent with the reported activity of Enoxacin to enhance DNA repair after DNA damage through boosting Dicer activity [80]. This activity was shown to involve the production of Dicer dependent non-coding RNAs called DNA damage response RNAs (DDRNAs) [81]. These data suggested that DNA damage is not the cause of the cell death induced by Aβ42 but a result of it. The separation of DNA damage and Aβ42 induced toxicity now allowed us to mechanistically interrogate the pathway of Aβ42 induced cell death and the role of the RNAi and DNA damage in it.

Tau has been shown to be required for Aβ42's toxicity in various models [55, 56]. To determine whether tau was also required in the cell death observed in SH cells when treated with Aβ42, we tested tau k.o. SH cells [82]. Interestingly, k.o. cells still differentiated normally (**Fig. 6f**). The two differentiated k.o. clones showed reduced sensitivity to Aβ42 induced toxicity and clone 231K (used in **Fig. 6f**) was almost completely resistant (**Fig. 6g**). As expected from the above data Aβ42 induced DNA damage was blocked in the tau k.o. cells (**Fig. 6h**). This analysis placed tau downstream of Aβ42 and upstream of cell death and DNA damage. To determine where DNA damage occurs with respect to the RISC activity, we pretreated Aβ42 exposed differentiated SH cells with 10 μM ATA. This ATA concentration which only reduced cell death by ~10% completely blocked DNA damage (**Fig. 6i**) and a similar finding was made when the Ago2 k.o. clones were tested (**Fig. 6h**). This places DNA damage downstream of the RISC and is consistent with our report showing that DISE inducing RNAi active sRNAs cause DNA damage in brain derived cells detectable in form of H2AX phosphorylation [20]. In summary, together our data suggest that DISE contributes to the pathology of AD initiated by the main mediator of AD, toxic Aβ oligomers. With an involvement of tau the RISC is engaged enhancing the toxic activity of Aβ42 through shifting the balance of RISC bound sRNAs to more toxic seeds. This contributes to DISE and DNA damage and together with RISC independent pathways causes neuronal dysfunction and neurodegeneration.

Discussion

DISE was discovered as a powerful cell death mechanism [52]. Our analysis of R-sRNAs in various AD models now supports DISE as a new concept of cell fate regulation that may affect the survival of neurons. While our analysis included any sRNA that can enter the RISC, in most cells including neurons >95% of the RISC content are miRNAs. The role of miRNAs in AD has been intensively studied [83, 84]. Most analyses on AD associated miRNAs are based on quantifying miRNAs from total small RNA fraction and different miRNAs have been associated with the disease [83, 84]. However, we and others have found that miRNAs vary dramatically in their ability to be taken up by the RISC [22, 85]. We therefore decided to subject various *in vitro* and *in vivo* systems to an analysis of RISC bound sRNAs. We chose an Ago-RP-Seq method rather than a method involving cross-linking miRNAs with their targets, as we were not per se interested in identifying miRNA targets. We provide data on DISE contributing to the neurotoxicity seen in AD.

In vitro experiments confirmed a contribution of the RISC and RNAi to the toxicity of Aβ42. In addition, we found a significant association between the level of neurotoxicity and the seed viability of R-sRNAs in different models of AD. Lower seed viability correlated with higher levels of cell death. Correspondingly, a higher overall seed viability of the RISC content may protect neurons from dying. Seed viability was lower in older mouse brains and in *in vitro* aged iPSC derived neurons suggesting a loss of protective miRNAs with age.

There is ample literature to support the notion that miRNAs are neuroprotective in a number of disease models: In *Drosophila* impairing miRNA processing dramatically enhanced neurodegeneration caused by the CAG repeat gene ATXN3 [86]. We previously demonstrated how toxic CAG repeat-derived sRNAs cause cell death [29, 74]. Consistently, pathogenic ATXN3 with amplified CAG repeats showed strongly enhanced toxicity in HeLa cells after knockdown of Dicer [87]. Multiple publications on mice with a tissue specific knock-out of Dicer in brain cells showed that reducing Dicer triggers neuronal loss and causes behavioral abnormalities, followed by the premature death of the animals (see [66, 67]). Moreover, mice with a tissue specific deletion of Dicer in spinal motor neurons exhibit hallmarks of spinal muscular atrophy (SMA) with signs of denervation [88]. Interestingly, mice with a brain specific knock out of Ago2 (using the same promoter: CaMKII Cre) showed no toxicity in neurons [89] suggesting that it is not the general activity of miRNAs and RNAi that is required for survival of neurons.

Conversely, increasing miRNAs levels can be neuroprotective. Amyotrophic Lateral Sclerosis (ALS) disease mice treated with Enoxacin [90], showed reduced disease scores [91]. In addition, it was directly shown that miRNAs in Dicer knockout mice protect adult dopamine neurons from neurotoxicity [79] and Enoxacin treatment promoted survival of cultured DA neurons. Enoxacin could have two beneficial effects, it may increase the amount of protective miRNAs [78] and boost DNA damage repair [80].

Based on our data we are now proposing a model with the RISC as a central rheostat affecting neuronal cell death and DNA damage during aging observed in AD with implications for other neurodegenerative diseases:

In young, normal or asymptomatic individuals the RISC is filled with abundant miRNAs, most of which contain nontoxic seeds and act as protectors, preventing large amounts of small RNAs (including rRNA and tRNA fragments) that carry G and C-rich regions and can be toxic through DISE from entering the RISC (**Fig. 7a**). tRNA and rRNA fragments have been reported to be increased in the brain of AD patients [92]. miRNAs may play at least two fundamental roles in this context: First, they act as signal regulators by targeting hundreds of genes, mostly involved in development and differentiation. Second, they are expressed at high levels preventing access of toxic endogenous sRNAs to the RISC.

In AD patients once they get older Aβ oligomers can elicit a cellular response that causes upregulation of endogenous toxic sRNAs (**Fig. 7b**). Mechanistically, our data suggest a moderate but significant contribution of DISE to the cell death seen in cells exposed to toxic Aβ42. We saw ~10% protection from Aβ42 induced cell death in cells with ATA inhibited Ago2 and after knock-out of Ago2. We also saw a ~10% sensitization of Drosha k.o. cells lacking protective miRNAs and this sensitization could be reversed by adding back some of the protective miRNAs most downregulated in the k.o. cells. In contrast, knock-out of tau had a much more fundamental effect and very substantially protected cells from cell death induced by Aβ42. These findings suggest that tau is required for Aβ42 to engage the RISC and to mediate toxicity, however, DNA damage caused by Aβ42 treatment seems to be entirely dependent on RISC engagement at least in the cell systems we used. Blocking or reversing DNA damage by Enoxacin treatment did not rescue cells from cell death suggesting the existence of pathway(s) that are parallel to DISE.

With increasing age the balance of R-sRNAs with toxic versus nontoxic seeds shifts towards lower seed viability rendering neurons susceptible to DISE inducing sRNAs. The age dependent loss of protective miRNAs may be due to a reduced ability of aging neurons to produce enough protective miRNAs. How could the amount of protective miRNAs be regulated during AD and ageing? The stability of Dicer which is critical to miRNA expression in the brain is sensitive to ROS and interferons (IFNs) which are both elevated during AD [93, 94] and

most of its expression in the brain is lost during aging [68]. In addition, it was recently shown that the highest Drosha expression in the brain is found in pyramidal neurons in the *Cornu Ammonis* (CA1-3) regions in the hippocampus and that during AD stress such as elevated ROS activates p38 MAPK which phosphorylates Drosha [95] in turn resulting in its translocation from the nucleus to the cytosol [96]. This should also result in a loss of most miRNAs similar to what we found in Drosha k.o. NB7 cells.

Our data point at two responses of cells to Aβ42 that involved RISC activity: Cell death/DISE and DNA damage (**Fig. 7b**). While cell death is a component of AD, it is thought to be a relatively late event in the collection of cascades that ultimately result in symptoms. That is why many in the field do not consider cell death as being essential. However, in all models of neuronal dysfunction, whether it is hyperactivity or neuronal silence resulting in cognitive impairment, neuronal dysfunction may also lead to cell death [97]. In a large and unique cell type such as a post-mitotic neuron, the disease can even affect cellular substructures as shown for developing axons due to a local activation of the RNAi machinery [98]. When patients die, they have lost a substantial amount of their brain cells.

DNA damage is seen in AD and it is accelerated during aging [6] and mutations increase in single AD neurons [7]. Based on our data the DISE mechanism may not only contribute to neuronal cell death but also to neurodegeneration by inducing DNA damage. Future experiments will have to determine to what extent engagement of the DISE mechanism contributes to synaptic dysfunction and neurodegeneration and the pathology of AD.

Increase in toxic sRNAs in the context of gradual loss of protective miRNAs during aging could also be at the core of other degenerative diseases that affect the brain such as Parkinson's disease (PD), Huntington's disease (HD), and ALS. As this loss in humans likely occurs over decades, this would explain why so many neurodegenerative diseases have an onset during adulthood with decades of symptom-free life. While the genetic modifiers and the triggers of DISE will likely be different in each of these diseases, the mechanism to protect cells from toxic sRNAs may be shared. Also, various forms of cell death have been described to occur in all of these diseases [99], however, as DISE is a combination of multiple cell death pathways depending on the transcriptome in the affected cells [20], some of these observed forms of cell death may be caused by cells undergoing DISE.

In summary, an age dependent loss of protective miRNAs together with the upregulation or the presence of toxic sRNAs combined with numerous genetic modifiers and genetic mutations present in familial and sporadic AD may contribute to AD.

Conclusions

The overwhelming investment in AD drug discovery has been focused on two mechanisms: 1) Reducing amyloid plaque load in the brain (the hallmark of AD diagnosis; 70-80% of the effort) and 2) preventing tau phosphorylation. However, treatments aimed at reducing amyloid plaque burden have not yet resulted in an effective treatment of AD (summarized in [100]). Our data support a hypothesis that high expression of nontoxic miRNAs protects from neurodegeneration and that increasing miRNA biogenesis or blocking toxic R-sRNAs may be a viable treatment option for many neurodegenerative diseases including AD.

Abbreviations

3'UTR: 3' untranslated region; Aβ: Amyloid-β; Ab42: 1-42 Aβ peptide; AD: Ago: Argonaute; Ago-RP-Seq: Ago RNA precipitation combined with small RNAseq; Alzheimer's disease; ATA: aurintricarboxylic acid; BDNF: neurotrophic factor; DISE: death induced by survival gene elimination; FAD: familial form of AD; iPSC: Induced pluripotent stem cells; k.o.: knockout; NFT: neurofibrillary tangles; p-tau: phosphorylated tau; RA: retinoic acid; RISC: RNA induced silencing complex; RNAi: RNA interferences; SH: SH-SY5Y cells; sRNA: short RNA; R-sRNA: RISC bound sRNA; siRNA: Small interfering RNA; miRNA: microRNA; TNR: trinucleotide repeat; wt: Wild-type.

Supplementary Information

The online version contains supplementary material available at

Acknowledgements

We would like to thank Drs. William Klein and Ruth Itzhaki for helpful discussions and input early in the project and Dr. Paolo Paganelli for proving tau knock-out SH-SY5Y cells.

Author's contributions
MP designed experiments, analyzed data, and conceptualized the work. BP designed, performed, and analyzed most of the *in vitro* experiments and BP and S-YJ performed the Ago-RP-Seq experiments. C-PM and AR stained and imaged mouse brains. AHL generated and characterized the Drosha k.o. NB7 cells. EB developed SPOROS and EB and BP performed bioinformatics analyses. KF and AF generated and cultured human iPSC derived neurons. JK and JM provided iPSC-derived neurons and their characterizing data. AM provided conceptual input. ER and CG provided the CN and SuperAger brain samples. AF provided brains from tau transgenic mice. BH and DG provided the brains of 5XFAD and 5XFAD Rubicon k.o. mice and BH performed the TUNEL staining of these brains. KS and RV provided training and input on working with AD brains. MP and BP wrote, and RV, AHK, BP, and MP edited the manuscript. All authors read and approved the final manuscript.

Funding
This work was supported by National Institutes of Health grants R01NS090993 (to A.F.), R01AG030142 (to R.V.), R01AG045571, R56AG045571, R01AG067781, U19AG073153, P30AG072977, P30AG13854 (to E.R. and C.G.), R01NS124783, and L40CA231423 (to B.L.H). The content is solely the responsibility of the authors and does not necessarily represent the official views of the National Institutes of Health. Further support was provided by the McKnight Brain Research Foundation (to E.R.).

Availability of data and materials
RNA seq data were deposited at GEO under accession number GSE213138 (https://www.ncbi.nlm.nih.gov/geo/query/acc.cgi?acc=GSE213138, reviewer token: ubkpguccdlsplwz). All other data generated and analyzed during this study are included in this published article and its supplementary information files.

Declarations
Ethics approval and consent to participate
All animal experiments were approved and conducted in accordance with IACUC regulations at Northwestern University, St. Jude's Children’s Hospital and University of South Florida, Tampa.

Consent for publication
Not applicable.

Competing interests
The authors declare that they have no competing interests.

References

1. Hardy JA, Higgins GA. Alzheimer's disease: the amyloid cascade hypothesis. *Science* **256**, 184-185 (1992).

2. Bhat AH*, et al.* Oxidative stress, mitochondrial dysfunction and neurodegenerative diseases; a mechanistic insight. *Biomed Pharmacother* **74**, 101-110 (2015).

3. Dawson TM, Dawson VL. Mitochondrial Mechanisms of Neuronal Cell Death: Potential Therapeutics. *Annu Rev Pharmacol Toxicol* **57**, 437-454 (2017).

4. Younkin SG. The role of A beta 42 in Alzheimer's disease. *J Physiol Paris* **92**, 289-292 (1998).

5. Hutton M, Perez-Tur J, Hardy J. Genetics of Alzheimer's disease. *Essays Biochem* **33**, 117-131 (1998).

6. Wang H, Lautrup S, Caponio D, Zhang J, Fang EF. DNA Damage-Induced Neurodegeneration in Accelerated Ageing and Alzheimer's Disease. *Int J Mol Sci* **22**, 6748 (2021).

7. Miller MB*, et al.* Somatic genomic changes in single Alzheimer's disease neurons. *Nature* **604**, 714-722 (2022).

8. Lewis BP, Shih IH, Jones-Rhoades MW, Bartel DP, Burge CB. Prediction of mammalian microRNA targets. *Cell* **115**, 787-798 (2003).

9. Lai EC. Micro RNAs are complementary to 3' UTR sequence motifs that mediate negative post-transcriptional regulation. *Nat Genet* **30**, 363-364 (2002).

10. Eulalio A, Huntzinger E, Izaurralde E. GW182 interaction with Argonaute is essential for miRNA-mediated translational repression and mRNA decay. *Nat Struct Mol Biol* **15**, 346-353 (2008).

11. Lee Y*, et al.* MicroRNA genes are transcribed by RNA polymerase II. *EMBO J* **23**, 4051-4060 (2004).

12. Han J, Lee Y, Yeom KH, Kim YK, Jin H, Kim VN. The Drosha-DGCR8 complex in primary microRNA processing. *Genes Dev* **18**, 3016-3027 (2004).

13. Yi R, Qin Y, Macara IG, Cullen BR. Exportin-5 mediates the nuclear export of pre-microRNAs and short hairpin RNAs. *Genes Dev* **17**, 3011-3016 (2003).

14. Bernstein E, Caudy AA, Hammond SM, Hannon GJ. Role for a bidentate ribonuclease in the initiation step of RNA interference. *Nature* **409**, 363-366 (2001).

15. Hutvagner G, McLachlan J, Pasquinelli AE, Balint E, Tuschl T, Zamore PD. A cellular function for the RNA-interference enzyme Dicer in the maturation of the let-7 small temporal RNA. *Science* **293**, 834-838 (2001).

16. Wang Y, Sheng G, Juranek S, Tuschl T, Patel DJ. Structure of the guide-strand-containing argonaute silencing complex. *Nature* **456**, 209-213 (2008).

17. Kim YK, Kim B, Kim VN. Re-evaluation of the roles of DROSHA, Exportin 5, and DICER in microRNA biogenesis. *Proc Natl Acad Sci U S A* **113**, E1881-1889 (2016).

18. Gao QQ*, et al.* 6mer seed toxicity in tumor suppressive miRNAs. *Nature Comm* **9**, 4504 (2018).

19. Patel M*, et al.* Identification of the toxic 6mer seed consensus in human cancer cells. *Sci Rep* **12**, 5130 (2022).

20. Hadji A*, et al.* Death induced by CD95 or CD95 ligand elimination. *Cell Rep* **7**, 208-222 (2014).

21. Putzbach W*, et al.* Many si/shRNAs can kill cancer cells by targeting multiple survival genes through an off-target mechanism. *eLife* **6**, e29702 (2017).

22. Patel M*, et al.* The ratio of toxic-to-nontoxic microRNAs predicts platinum sensitivity in ovarian cancer. *Cancer Res* **81**, 3985-4000 (2021).

23. Murmann AE, Bartom ET, Schipma MJ, Vilker J, Chen S, Peter ME. 6mer seed toxicity in viral microRNAs. *iScience* **23**, 100737 (2019).

24. Karanth SD*, et al.* Cancer diagnosis is associated with a lower burden of dementia and less Alzheimer's-type neuropathology. *Brain* **145**, 2518-2527 (2022).

25. Musicco M*, et al.* Inverse occurrence of cancer and Alzheimer disease: a population-based incidence study. *Neurology* **81**, 322-328 (2013).

26. Majd S, Power J, Majd Z. Alzheimer's Disease and Cancer: When Two Monsters Cannot Be Together. *Front Neurosci* **13**, 155 (2019).

27. Fa M, Orozco IJ, Francis YI, Saeed F, Gong Y, Arancio O. Preparation of oligomeric beta-amyloid 1-42 and induction of synaptic plasticity impairment on hippocampal slices. *J Vis Exp* **41**, 1884 (2010).

28. Stine WB, Jungbauer L, Yu C, LaDu MJ. Preparing synthetic Abeta in different aggregation states. *Methods Mol Biol* **670**, 13-32 (2011).

29. Murmann AE*, et al.* Small interfering RNAs based on huntingtin trinucleotide repeats are highly toxic to cancer cells. *EMBO Rep* **19**, e45336 (2018).

30. Krishtal J, Metsla K, Bragina O, Tõugu V, Palumaa P. Toxicity of Amyloid-β Peptides Varies Depending on Differentiation Route of SH-SY5Y Cells. *J Alzheimers Dis* **71**, 879-887 (2019).

31. Encinas M*, et al.* Sequential treatment of SH-SY5Y cells with retinoic acid and brain-derived neurotrophic factor gives rise to fully differentiated, neurotrophic factor-dependent, human neuron-like cells. *J Neurochem* **75**, 991-1003 (2000).

32. Tagai N, Tanaka A, Sato A, Uchiumi F, Tanuma SI. Low Levels of Brain-Derived Neurotrophic Factor Trigger Self-aggregated Amyloid β-Induced Neuronal Cell Death in an Alzheimer's Cell Model. *Biol Pharm Bull* **43**, 1073-1080 (2020).

33. Oakley H*, et al.* Intraneuronal beta-amyloid aggregates, neurodegeneration, and neuron loss in transgenic mice with five familial Alzheimer's disease mutations: potential factors in amyloid plaque formation. *J Neurosci* **26**, 10129-10140 (2006).

34. Heckmann BL*, et al.* LC3-Associated Endocytosis Facilitates beta-Amyloid Clearance and Mitigates Neurodegeneration in Murine Alzheimer's Disease. *Cell* **178**, 536-551 e514 (2019).

35. Lang AE, Riherd Methner DN, Ferreira A. Neuronal degeneration, synaptic defects, and behavioral abnormalities in tau(4)(5)(-)(2)(3)(0) transgenic mice. *Neuroscience* **275**, 322-339 (2014).

36. McKhann GM*, et al.* The diagnosis of dementia due to Alzheimer's disease: recommendations from the National Institute on Aging-Alzheimer's Association workgroups on diagnostic guidelines for Alzheimer's disease. *Alzheimers Dement* **7**, 263-269 (2011).

37. Hyman BT*, et al.* National Institute on Aging-Alzheimer's Association guidelines for the neuropathologic assessment of Alzheimer's disease. *Alzheimers Dement* **8**, 1-13 (2012).

38. Rogalski EJ*, et al.* Youthful memory capacity in old brains: anatomic and genetic clues from the Northwestern SuperAging Project. *J Cogn Neurosci* **25**, 29-36 (2013).

39. Wadhwani AR, Affaneh A, Van Gulden S, Kessler JA. Neuronal apolipoprotein E4 increases cell death and phosphorylated tau release in alzheimer disease. *Ann Neurol* **85**, 726-739 (2019).

40. Zhang Y*, et al.* Rapid single-step induction of functional neurons from human pluripotent stem cells. *Neuron* **78**, 785-798 (2013).

41. Mazzulli JR, Zunke F, Isacson O, Studer L, Krainc D. alpha-Synuclein-induced lysosomal dysfunction occurs through disruptions in protein trafficking in human midbrain synucleinopathy models. *Proc Natl Acad Sci U S A* **113**, 1931-1936 (2016).

42. Hauptmann J*, et al.* Biochemical isolation of Argonaute protein complexes by Ago-APP. *Proc Natl Acad Sci U S A* **112**, 11841-11845 (2015).

43. Hafner M, Renwick N, Farazi TA, Mihailović A, Pena JTG, Tuschl T. Barcoded cDNA library preparation for small RNA profiling by next-generation sequencing. *Methods* **58**, 164-170 (2012).

44. Patel N*, et al.* MicroRNAs can regulate human APP levels. *Mol Neurodegener* **3**, 10 (2008).

45. Bartom ET*, et al.* SPOROS: A pipeline to analyze DISE/6mer seed toxicity. *PLOS Comp Biol* **18**, e1010022 (2021).

46. Feng MG*, et al.* MiR-21 attenuates apoptosis-triggered by amyloid-beta via modulating PDCD4/ PI3K/AKT/GSK-3beta pathway in SH-SY5Y cells. *Biomed Pharmacother* **101**, 1003-1007 (2018).

47. Higaki S*, et al.* Defensive effect of microRNA-200b/c against amyloid-beta peptide-induced toxicity in Alzheimer's disease models. *PLoS One* **13**, e0196929 (2018).

48. Lambert MP*, et al.* Beta/A4-evoked degeneration of differentiated SH-SY5Y human neuroblastoma cells. *J Neurosci Res* **39**, 377-385 (1994).

49. Krishtal J, Bragina O, Metsla K, Palumaa P, Tougu V. In situ fibrillizing amyloid-beta 1-42 induces neurite degeneration and apoptosis of differentiated SH-SY5Y cells. *PLoS One* **12**, e0186636 (2017).

50. Ferreira A, Busciglio J, Landa C, Caceres A. Ganglioside-enhanced neurite growth: evidence for a selective induction of high-molecular-weight MAP-2. *J Neurosci* **10**, 293-302 (1990).

51. Kaplan DR, Matsumoto K, Lucarelli E, Thiele CJ. Induction of TrkB by retinoic acid mediates biologic responsiveness to BDNF and differentiation of human neuroblastoma cells. Eukaryotic Signal Transduction Group. *Neuron* **11**, 321-331 (1993).

52. Haluck-Kangas A, Patel M, Paudel B, Vaidyanathan A, Murmann AE, Peter MP. DISE/6mer Seed Toxicity - A powerful anti-cancer mechanism with implications for other diseases. *J Exp Clin Cancer Res* **40**, 389 (2021).

53. Park H, Lee YB, Chang KA. miR-200c suppression increases tau hyperphosphorylation by targeting 14-3-3gamma in early stage of 5xFAD mouse model of Alzheimer's disease. *Int J Biol Sci* **18**, 2220-2234 (2022).

54. Martinez J*, et al.* Molecular characterization of LC3-associated phagocytosis reveals distinct roles for Rubicon, NOX2 and autophagy proteins. *Nat Cell Biol* **17**, 893-906 (2015).

55. Roberson ED*, et al.* Reducing endogenous tau ameliorates amyloid beta-induced deficits in an Alzheimer's disease mouse model. *Science* **316**, 750-754 (2007).

56. Rapoport M, Dawson HN, Binder LI, Vitek MP, Ferreira A. Tau is essential to beta -amyloid-induced neurotoxicity. *Proc Natl Acad Sci U S A* **99**, 6364-6369 (2002).

57. Ferreira A, Bigio EH. Calpain-mediated tau cleavage: a mechanism leading to neurodegeneration shared by multiple tauopathies. *Mol Med* **17**, 676-685 (2011).

58. Hernandez F, Merchan-Rubira J, Valles-Saiz L, Rodriguez-Matellan A, Avila J. Differences Between Human and Murine Tau at the N-terminal End. *Front Aging Neurosci* **12**, 11 (2020).

59. Afreen S, Ferreira A. The formation of small aggregates contributes to the neurotoxic effects of tau(45-230). *Neurochem Int* **152**, 105252 (2022).

60. Sethi P, Lukiw WJ. Micro-RNA abundance and stability in human brain: Specific alterations in Alzheimer's disease temporal lobe neocortex. *Neuroscience Letters* **459**, 100-104 (2009).

61. Chen ML*, et al.* Inhibition of miR-331-3p and miR-9-5p ameliorates Alzheimer's disease by enhancing autophagy. *Theranostics* **11**, 2395-2409 (2021).

62. Rossi RL*, et al.* Distinct microRNA signatures in human lymphocyte subsets and enforcement of the naive state in CD4+ T cells by the microRNA miR-125b. *Nat Immunol* **12**, 796-803 (2011).

63. Roy S. miRNA in Macrophage Development and Function. *Antioxid Redox Signal* **25**, 795-804 (2016).

64. Jovicic A*, et al.* Comprehensive expression analyses of neural cell-type-specific miRNAs identify new determinants of the specification and maintenance of neuronal phenotypes. *J Neurosci* **33**, 5127-5137 (2013).

65. Kosik KS. The neuronal microRNA system. *Nat Rev Neurosci* **7**, 911-920 (2006).

66. Schaefer A*, et al.* Cerebellar neurodegeneration in the absence of microRNAs. *J Exp Med* **204**, 1553-1558 (2007).

67. Davis TH*, et al.* Conditional loss of Dicer disrupts cellular and tissue morphogenesis in the cortex and hippocampus. *J Neurosci* **28**, 4322-4330 (2008).

68. Mori MA*, et al.* Role of microRNA processing in adipose tissue in stress defense and longevity. *Cell Metab* **16**, 336-347 (2012).

69. Mertens J, Reid D, Lau S, Kim Y, Gage FH. Aging in a Dish: iPSC-Derived and Directly Induced Neurons for Studying Brain Aging and Age-Related Neurodegenerative Diseases. *Annu Rev Genet* **52**, 271-293 (2018).

70. Min KW*, et al.* Profiling of m6A RNA modifications identified an age-associated regulation of AGO2 mRNA stability. *Aging Cell* **17**, e12753 (2018).

71. Putzbach W*, et al.* CD95/Fas ligand mRNA is toxic to cells. *eLife* **7**, e38621 (2018).

72. Vaidyanathan A*, et al.* Analysis of the contribution of 6mer seed toxicity to HIV-1 induced cytopathicity. *J Virol*, In press (2022).

73. Tan GS, Chiu CH, Garchow BG, Metzler D, Diamond SL, Kiriakidou M. Small molecule inhibition of RISC loading. *ACS Chem Biol* **7**, 403-410 (2012).

74. Murmann AE, Patel M, Jeong SY, Bartom ET, Morton AJ, Peter ME. The length of uninterrupted CAG repeats in stem regions of repeat disease associated hairpins determines the amount of short CAG oligonucleotides that are toxic to cells through RNA interference. *Cell Death Dis* **13**, 1078 (2022).

75. Hallick RB, Chelm BK, Gray PW, Orozco EM, Jr. Use of aurintricarboxylic acid as an inhibitor of nucleases during nucleic acid isolation. *Nucleic Acids Res* **4**, 3055-3064 (1977).

76. Loo DT, Copani A, Pike CJ, Whittemore ER, Walencewicz AJ, Cotman CW. Apoptosis is induced by beta-amyloid in cultured central nervous system neurons. *Proc Natl Acad Sci U S A* **90**, 7951-7955 (1993).

77. Shan G*, et al.* A small molecule enhances RNA interference and promotes microRNA processing. *Nat Biotechnol* **26**, 933-940 (2008).

78. Melo S*, et al.* Small molecule enoxacin is a cancer-specific growth inhibitor that acts by enhancing TAR RNA-binding protein 2-mediated microRNA processing. *Proc Natl Acad Sci U S A* **108**, 4394-4399 (2011).

79. Chmielarz P*, et al.* Dicer and microRNAs protect adult dopamine neurons. *Cell Death Dis* **8**, e2813 (2017).

80. Gioia U*, et al.* Pharmacological boost of DNA damage response and repair by enhanced biogenesis of DNA damage response RNAs. *Sci Rep* **9**, 6460 (2019).

81. Francia S*, et al.* Site-specific DICER and DROSHA RNA products control the DNA-damage response. *Nature* **488**, 231-235 (2012).

82. Sola M*, et al.* Tau affects P53 function and cell fate during the DNA damage response. *Commun Biol* **3**, 245 (2020).

83. Pan Y*, et al.* Dysregulation and diagnostic potential of microRNA in Alzheimer's disease. *J Alzheimers Dis* **49**, 1-12 (2016).

84. Samadian M, Gholipour M, Hajiesmaeili M, Taheri M, Ghafouri-Fard S. The Eminent Role of microRNAs in the Pathogenesis of Alzheimer's Disease. *Front Aging Neurosci* **13**, 641080 (2021).

85. Flores O, Kennedy EM, Skalsky RL, Cullen BR. Differential RISC association of endogenous human microRNAs predicts their inhibitory potential. *Nucleic Acids Res* **42**, 4629-4639 (2014).

86. Jiang F, Ye X, Liu X, Fincher L, McKearin D, Liu Q. Dicer-1 and R3D1-L catalyze microRNA maturation in Drosophila. *Genes Dev* **19**, 1674-1679 (2005).

87. Bilen J, Liu N, Burnett BG, Pittman RN, Bonini NM. MicroRNA pathways modulate polyglutamine-induced neurodegeneration. *Mol Cell* **24**, 157-163 (2006).

88. Haramati S*, et al.* miRNA malfunction causes spinal motor neuron disease. *Proc Natl Acad Sci U S A* **107**, 13111-13116 (2010).

89. Schaefer A*, et al.* Argonaute 2 in dopamine 2 receptor-expressing neurons regulates cocaine addiction. *J Exp Med* **207**, 1843-1851 (2010).

90. Bailey RR, Peddie BA. Enoxacin for the treatment of urinary tract infection. *N Z Med J* **98**, 286-288 (1985).

91. Emde A*, et al.* Dysregulated miRNA biogenesis downstream of cellular stress and ALS-causing mutations: a new mechanism for ALS. *EMBO J* **34**, 2633-2651 (2015).

92. Wu W, Lee I, Spratt H, Fang X, Bao X. tRNA-Derived Fragments in Alzheimer's Disease: Implications for New Disease Biomarkers and Neuropathological Mechanisms. *J Alzheimers Dis* **79**, 793-806 (2021).

93. Wiesen JL, Tomasi TB. Dicer is regulated by cellular stresses and interferons. *Mol Immunol* **46**, 1222-1228 (2009).

94. Machitani M, Sakurai F, Wakabayashi K, Takayama K, Tachibana M, Mizuguchi H. Type I Interferons Impede Short Hairpin RNA-Mediated RNAi via Inhibition of Dicer-Mediated Processing to Small Interfering RNA. *Mol Ther Nucleic Acids* **6**, 173-182 (2017).

95. Yang Q*, et al.* Stress induces p38 MAPK-mediated phosphorylation and inhibition of Drosha-dependent cell survival. *Mol Cell* **57**, 721-734 (2015).

96. Xu H*, et al.* p38 MAPK-mediated loss of nuclear RNase III enzyme Drosha underlies amyloid beta-induced neuronal stress in Alzheimer's disease. *Aging Cell* **20**, e13434 (2021).

97. Zott B, Busche MA, Sperling RA, Konnerth A. What Happens with the Circuit in Alzheimer's Disease in Mice and Humans? *Annu Rev Neurosci* **41**, 277-297 (2018).

98. Hengst U, Cox LJ, Macosko EZ, Jaffrey SR. Functional and selective RNA interference in developing axons and growth cones. *J Neurosci* **26**, 5727-5732 (2006).

99. Moujalled D, Strasser A, Liddell JR. Molecular mechanisms of cell death in neurological diseases. *Cell Death Differ* **28**, 2029-2044 (2021).

100. Khachaturian AS*, et al.* Future prospects and challenges for Alzheimer's disease drug development in the era of the NIA-AA Research Framework. *Alzheimers Dement* **14**, 532-534 (2018).

Figure legends

Fig. 1 | Exposure of differentiated SH cells to Aβ42 results in a shift in R-sRNAs with lower seed viability. **a** Phase contrast image of undifferentiated SH cells or SH cells differentiated with RA/BDNF for 7 days. Size bar = 60 μm. **b** Western blot analysis of cells in **a**. **c** Viability of undifferentiated or 7 day differentiated SH cells treated with either Aβ40 or Aβ42 for 24 or 48 hrs. Data were normalized to the 24 hr treatment with Aβ40. **d** Scheme illustrating how the ratio of RISC bound sRNAs with nontoxic (green) versus toxic seeds (red) can protect cells from DISE. **e** Difference in seed viability of R-sRNAs significantly ($p<0.05$) under- or overrepresented in 7 day differentiated SH cells treated with Aβ42 for different periods of times (compared to Aβ40 treated cells). Shown are the medians and Kruskal-Wallis median test p-values.

Fig. 2 | Reduction in seed viability of R-sRNAs in AD mouse models with neurotoxicity. **a** Representative TUNEL staining of brains of 6-month-old control ($5XFAD^{Neg}$/$Rubicon^{+/-}$ and $5XFAD^{Neg}$/$Rubicon^{-/-}$), 5XFAD tg ($5XFAD^{TG}$/$Rubicon^{+/-}$), and $5XFAD^{TG}$/$Rubicon^{-/-}$ mice. Brain sections were counterstained with DAPI. Size marker = 200 μm. **b** Quantification of TUNEL positivity in brains of mice with four different genotypes. Top, 6-months and bottom, 8-month-old mice. Student's T-test p-values are given. ns, not significant. **c**, **d** Seed viability graphs of differentially expressed R-sRNAs ($p<0.05$) between 5XFAD $Rubicon^{+/-}$ (Het) and 5XFAD $Rubicon^{-/-}$ (**c**) and control and tau_{45-230} transgenic mouse (**d**) brains. miRNAs are labeled that have a difference in expression of 1000 or more reads. Enriched sRNAs are shown in green and depleted sRNAs in red. Shown are averages of triplicate (**c**) or quadruplicate (**d**) samples. Inserts: Seed viability plots of the seed viability of the same samples. Shown are the median viability of opposing differentially expressed and/or RISC-loaded sRNAs. Kruskal-Wallis median test p-value are given.

Fig. 3 | Reduced seed viability of R-sRNAs in iPSC derived neurons from AD patients. **a** Bright field image of the NGN2 excitatory neurons derived from two control and two AD patients 36 days post differentiation. Size bar = 500 μm. **b** Immunofluorescence images of the AD derived neurons using the neuronal marker βiiiTubulin and the glutamatergic neuronal marker vesicular glutamate transporter (vGLUT) counterstained with DAPI. Size bar = 50 μm. **c** Western blot analysis of Ctr (NUAD0635) and AD (AG5810) iPSC derived neurons. The analysis was done with half of the cells that were subjected to the Ago-RP-Seq-SPOROS analysis. **d** Seed viability graph of total R-sRNAs of the two Ctr and two AD patient derived iPSC derived neurons (average for each set is shown). Shown are averages of duplicate samples. sRNAs with 10,000 or more reads in at least one sample are labeled. In each label sRNAs are listed in the order of expression levels. **e** Seed viability plot of the differential seed viability of the samples in A. Medians and Kruskal-Wallis median test p-value are given.

Fig. 4 | Changes in seed viability of R-sRNAs with age. **a** Seed viability graph of differentially expressed R-sRNAs of 2- and 18-month-old mouse brains. Shown are averages of triplicate samples. sRNAs that have a difference in expression of 1000 or more reads are labeled. Enriched sRNAs are shown in green and depleted sRNAs in red. Insert: Seed viability plot of the differential seed viability of the analysis. Medians and Kruskal-Wallis median test p-value are given. **b** Seed viability graph of total R-sRNAs of iPSC derived neurons aged for 1 and 5 months. sRNAs with 10,000 or more reads in at least one sample are labeled. In each label sRNAs are listed in the order of expression levels. Enriched sRNAs are shown in green and depleted sRNAs in red. Insert: Seed viability plot of the differential seed viability of the analysis. Medians and Kruskal-Wallis median test p-value are given. Western blot insert: Analysis of iPSC derived neurons aged in vitro for 30, 150 or 190 days. Densitometrical quantification relative to the 30-day time point and actin is given. **c** *Top*, Average seed viability of all significantly up- and downregulated miRNAs in PBMCs of old versus young donors [70]. *Bottom*, Nucleotide composition at each of the six seed positions in the miRNAs analyzed above. **c,** *Top*, Seed viability plots of the differential seed viability of postmortem CN and SuperAger brains. Age of the three CN participants: 100, 87, 83 - average = 90, age of the three SuperAgers: 82, 85, 90 - average = 85.7. Medians and Kruskal-Wallis median test p-value are given. *Bottom*, average seed composition of the sRNAs in the same samples.

Fig. 5 | Increasing the amount of miRNAs with nontoxic seeds lowers the sensitivity of cells to Aβ42 induced cell death. **a** Western blot analysis of parental NB7 cells and two Drosha k.o. clones. Par, parental. **b** Relative amounts of total RISC bound miRNAs of the cells in a. **c** Real-time PCR quantification of major miRNAs in the two k.o. clones relative to parental cells. Shown are averages with variance of samples done in duplicate (miR-221/miR-181) or SD of samples done in triplicate (Let-7a and miR-21). The data on miR-21 and Let-7a are representative of two biological replicates. **d** Viability assay of parental NB7 cells or two Drosha k.o. clones after a 48 hr treatment with Aβ40 or Aβ42. **e** Seed viability graph of all R-sRNAs sequenced in parental NB7 cells and

two Drosha k.o. clones. sRNAs with 10,000 or more reads in at least one sample are labeled. Enriched sRNAs are shown in green and depleted sRNAs in red. The peaks containing the most highly expressed and most downregulated miRNAs in the two k.o. clones are marked by a blue arrow. **f** Seed viability plots of the seed viability of the samples in **e**. Shown are the medians and Kruskal-Wallis median test p-value. **g** Average seed composition of all sRNAs in the three samples in **e**. **h** The top 10 most abundant RISC bound miRNAs in parental NB7 cells with their 6mer seed and seed viabilities (%) and their expression and expression changes in the two Drosha k.o. clones. The top three most abundant miRNAs (labeled in **e** with arrows) are highlighted in red. **i** Viability assay of differentiated SH cells treated for 72 hrs with 20 μM Aβ42 relative to cells treated with Aβ40 (stippled line). Cells were mock transfected (L) or transfected with a control sRNA modified to block RISC access, or different amounts either miR-21-5p (21), miR-25-3p (25), miR-92-3p (92) or a cocktail of the three miRNAs for 24 hrs. Total concentration for each miRNA or the cocktail is given. The cocktail contained equal amounts of the individual miRNAs. Mean with SD and Student's t-test p-values are shown (**d, i**). * $p<0.05$, ** $p<0.01$., *** $p<0.001$.

Fig. 6 | Dependence of Aβ42 induced cell death and DNA damage on an active RISC. a Viability assay of differentiated SH cells control treated for 72 hrs with either 10 μM Aβ40 or Aβ40 in the absence or presence of 10 μM ATA. **b** Western blot analysis of parental SH cells and three Ago2 k.o. clones. **c** Western blot analysis of undifferentiated or 7-day differentiated SH cells and two Ago2 k.o. clones. **d** Viability assay of three Ago2 k.o. SH clones after exposure to 20 μM Aβ40 or Aβ42 for 72 hrs. **e** *top*, Western blot analysis differentiated SH cells control treated or pretreated with different concentrations of Enoxacin for 24 hrs and then treated with either 20 μM Aβ40 or Aβ42 for 24 hrs. *Bottom*, viability assay of the same analysis but treated with Aβ40/42 for 72 hrs. **f** Western blot analysis of undifferentiated or 7-day differentiated parental SH cells or tau k.o. clone 231K. **g** Viability assay of differentiated parental SH cells or two tau k.o. clones after mock treatment or treatment with 20 μM Aβ40/42. **h** Western blot analysis of par SH cells or different k.o. clones treated with 20 μM Aβ40/42 for 24 hrs. **i** Western blot for γH2AX of 7 day differentiated SH cells treated with Aβ40 or Aβ42 for four hours in the absence or pretreated for 24 hrs with of 10 μM ATA. Mean with SD and Student's t-test p-values are shown (**a, d, g**). * $p<0.05$, *** $p<0.001$.

Fig. 7 | A model that connects DISE, DNA damage, AD, and aging. a The situation in normal or asymptomatic individuals at a young age. The ratio of nontoxic to toxic sRNAs that are bound to the RISC prevents cells from undergoing DISE. **b** The situation in older and symptomatic AD patients. Dicer expression is reduced with age resulting in a gradual reduction of protective miRNAs in turn causing a shift in RISC bound sRNAs to lower seed viability sensitizing cells to DISE and DNA damage. Tau mediates Aβ42 induced cell death in part through the RISC and DISE. In contrast, DNA damage induced by Aβ42/tau is dependent on RISC activity. RISC, RNA-induced silencing complex; DISE, death induced by survival gene elimination; sRNA; short RNA. Two inhibitors (blue) and their site of action are shown.

Figure 1

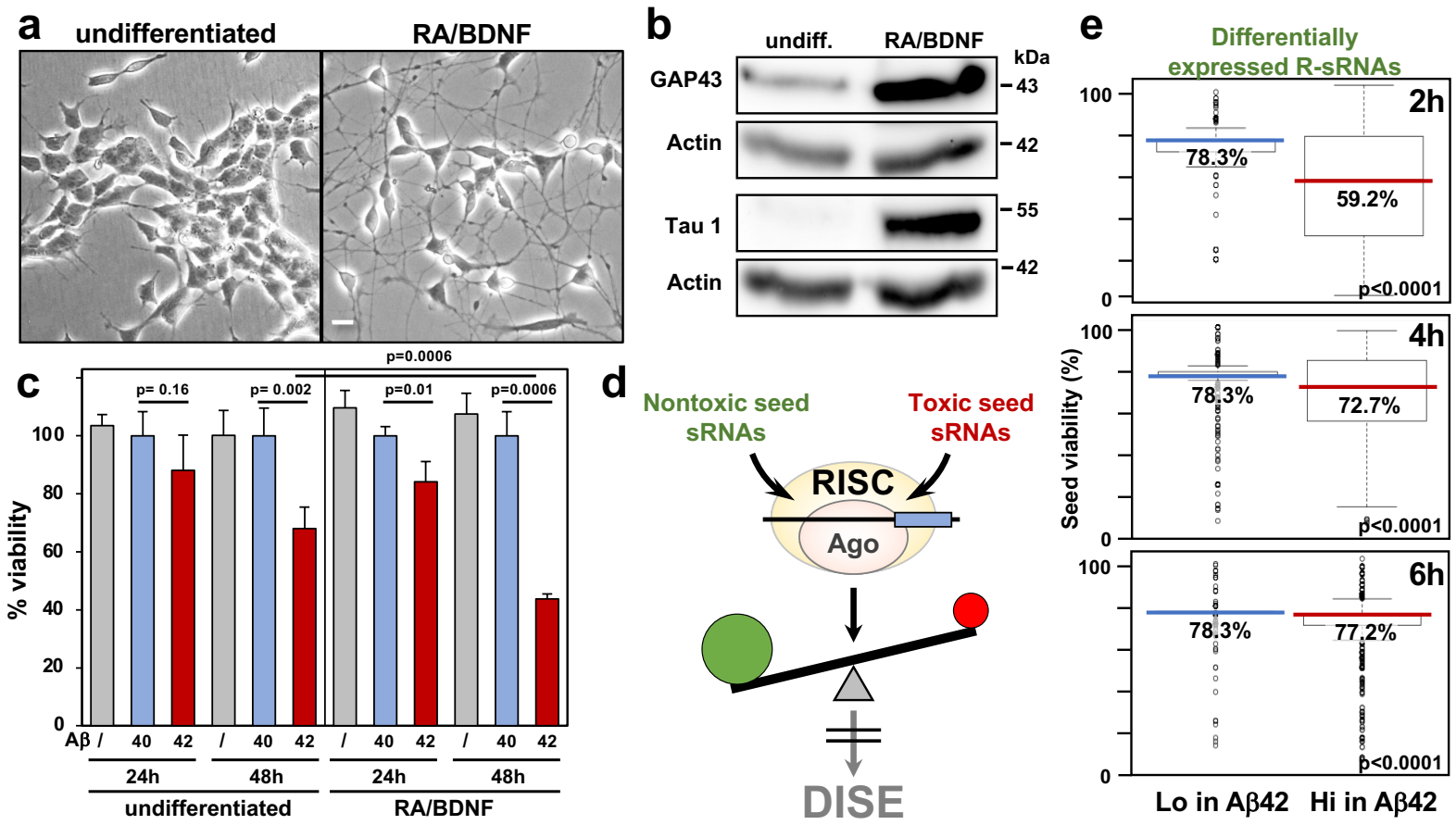
a
undifferentiated
RA/BDNF
b
undiff.
RA/BDNF
kDa
GAP43
43
Actin
42
Tau 1
55
Actin
42
c
p=0.0006
p= 0.16
p= 0.002
p=0.01
p=0.0006
% viability
100
80
60
40
20
0
Aβ / 40 42 / 40 42 / 40 42 / 40 42
24h
48h
24h
48h
undifferentiated
RA/BDNF
d
Nontoxic seed sRNAs
Toxic seed sRNAs
RISC
Ago
DISE
e
Differentially expressed R-sRNAs
2h
78.3%
59.2%
p<0.0001
4h
78.3%
72.7%
p<0.0001
6h
78.3%
77.2%
p<0.0001
Seed viability (%)
100
0
Lo in Aβ42
Hi in Aβ42

Figure 2

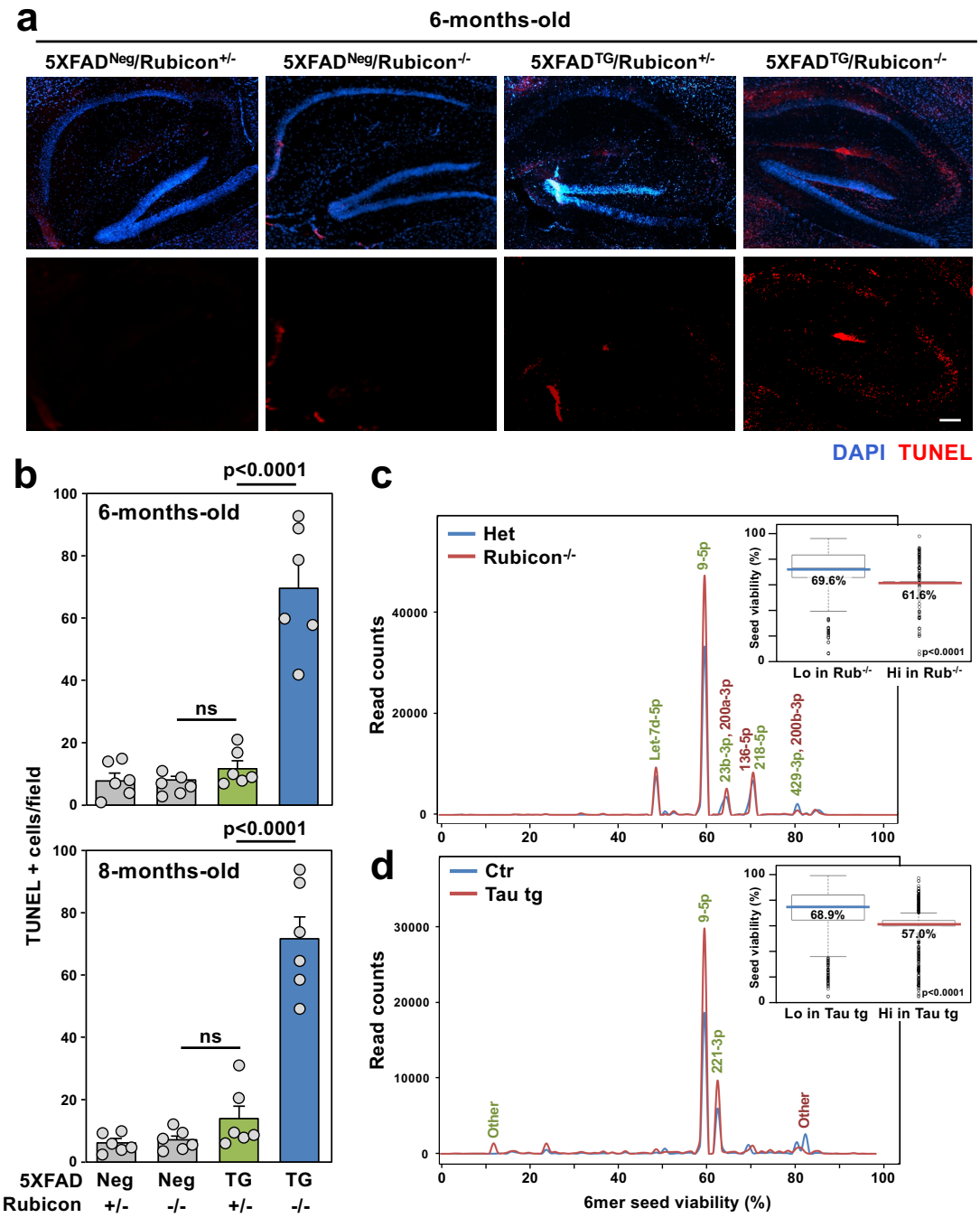
a
6-months-old
5XFAD^Neg/Rubicon^+/-
5XFAD^Neg/Rubicon^-/-
5XFAD^TG/Rubicon^+/-
5XFAD^TG/Rubicon^-/-
DAPI TUNEL
b
p<0.0001
6-months-old
ns
p<0.0001
8-months-old
ns
TUNEL + cells/field
5XFAD Neg Neg TG TG
Rubicon +/- -/- +/- -/-
c
Het
Rubicon-/-
Read counts
9-5p
Let-7d-5p
23b-3p, 200a-3p
136-5p
218-5p
429-3p, 200b-3p
Seed viability (%)
69.6%
61.6%
p<0.0001
Lo in Rub-/-
Hi in Rub-/-
d
Ctr
Tau tg
Read counts
9-5p
221-3p
Other
Other
Seed viability (%)
68.9%
57.0%
p<0.0001
Lo in Tau tg
Hi in Tau tg
6mer seed viability (%)

Figure 3

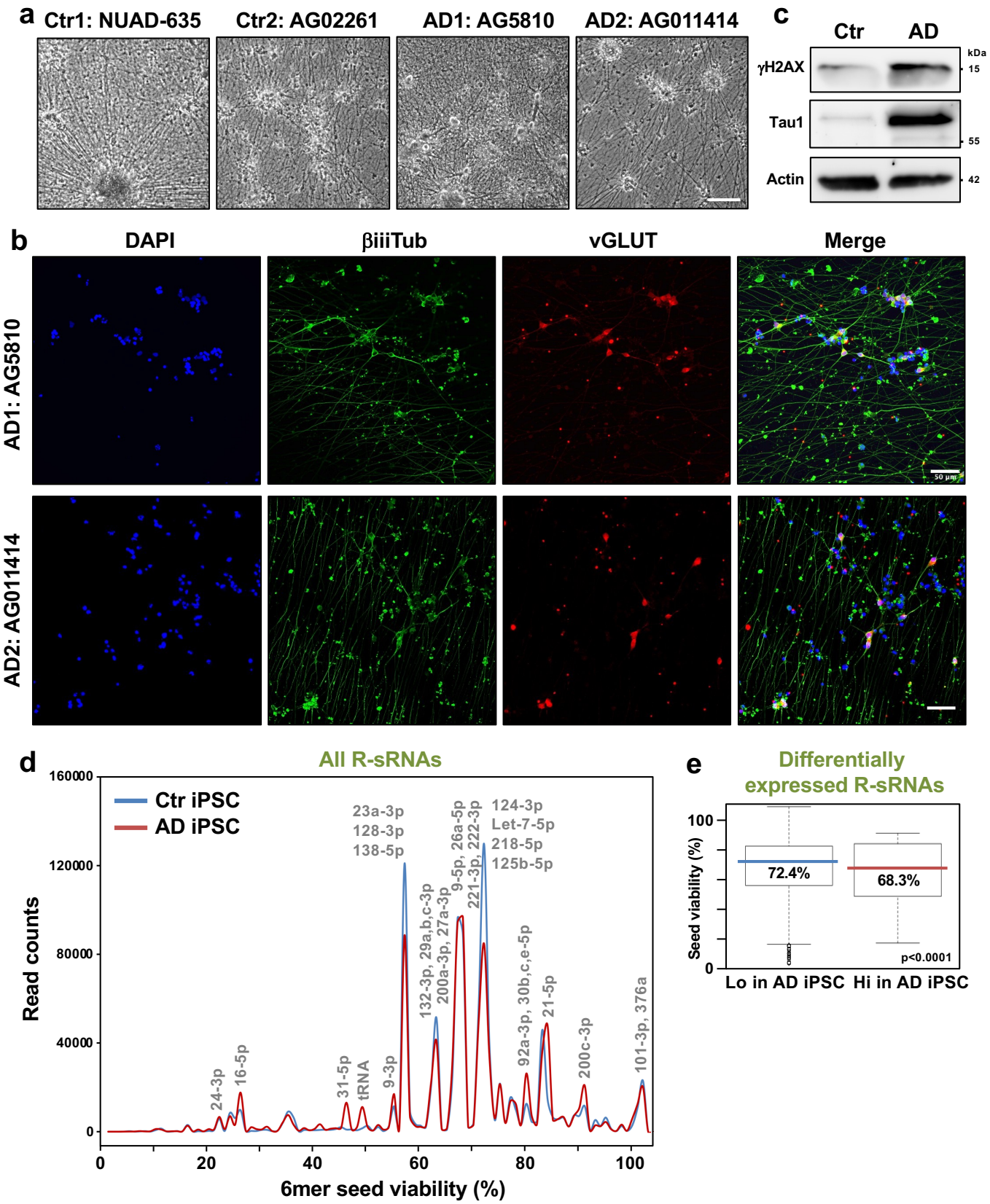
a
Ctr1: NUAD-635
Ctr2: AG02261
AD1: AG5810
AD2: AG011414
c
Ctr
AD
γH2AX
Tau1
Actin
kDa
15
55
42
b
DAPI
βiiiTub
vGLUT
Merge
AD1: AG5810
AD2: AG011414
50 µm
d
All R-sRNAs
Ctr iPSC
AD iPSC
Read counts
6mer seed viability (%)
160000
120000
80000
40000
0
20
40
60
80
100
24-3p
16-5p
31-5p
tRNA
9-3p
23a-3p
128-3p
138-5p
132-3p, 29a,b,c-3p
200a-3p, 27a-3p
9-5p, 26a-5p
221-3p, 222-3p
124-3p
Let-7-5p
218-5p
125b-5p
92a-3p, 30b,c,e-5p
21-5p
200c-3p
101-3p, 376a
e
Differentially expressed R-sRNAs
Seed viability (%)
72.4%
68.3%
p<0.0001
Lo in AD iPSC
Hi in AD iPSC

Figure 4

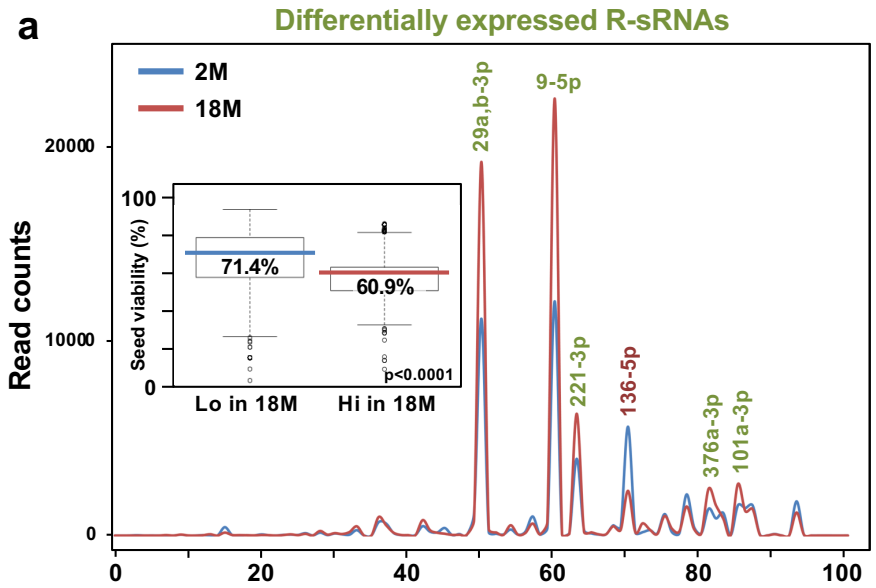
a
Differentially expressed R-sRNAs
2M
18M
Read counts
20000
10000
0
29a,b-3p
9-5p
221-3p
136-5p
376a-3p
101a-3p
Seed viability (%)
71.4%
60.9%
p<0.0001
Lo in 18M
Hi in 18M
0
20
40
60
80
100

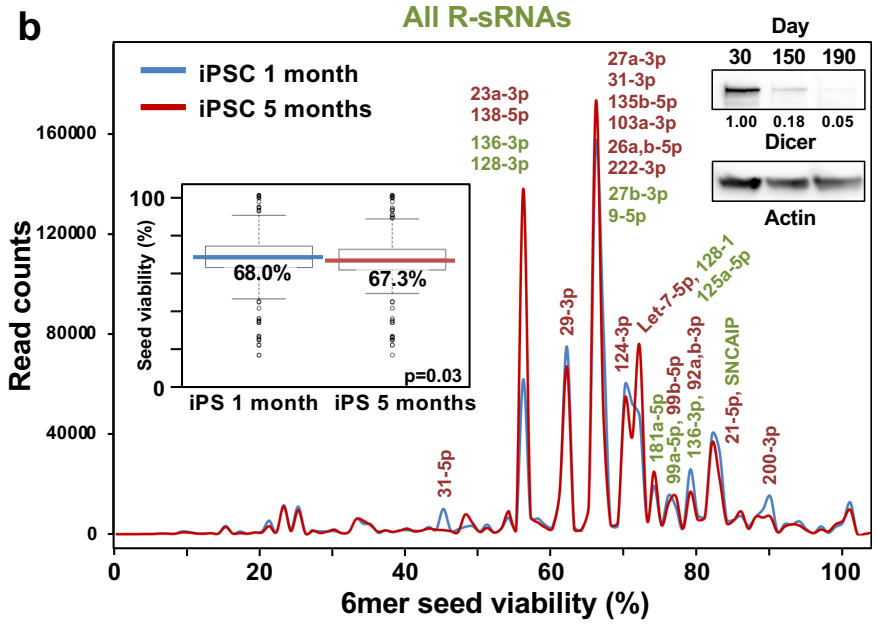
b
All R-sRNAs
iPSC 1 month
iPSC 5 months
Read counts
160000
120000
80000
40000
0
23a-3p
138-5p
136-3p
128-3p
27a-3p
31-3p
135b-5p
103a-3p
26a,b-5p
222-3p
27b-3p
9-5p
29-3p
124-3p
Let-7-5p, 128-1
125a-5p
181a-5p
99b-5p
99a-5p, 92a,b-3p
136-3p, 21-5p, SNCAIP
200-3p
31-5p
Day
30
150
190
1.00
0.18
0.05
Dicer
Actin
Seed viability (%)
68.0%
67.3%
p=0.03
iPS 1 month
iPS 5 months
6mer seed viability (%)

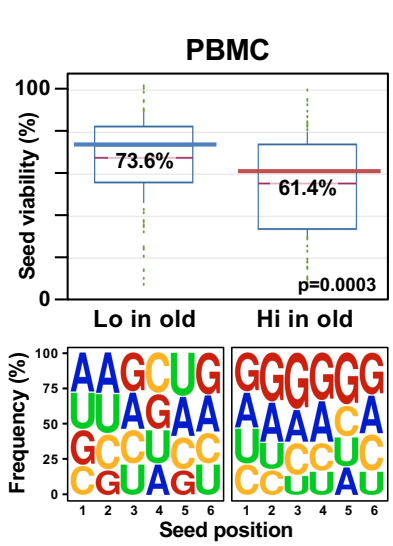
c
PBMC
Seed viability (%)
73.6%
61.4%
p=0.0003
Lo in old
Hi in old
Frequency (%)
Seed position

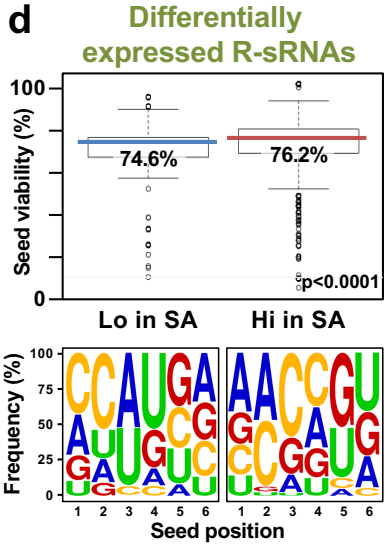
d
Differentially expressed R-sRNAs
Seed viability (%)
74.6%
76.2%
p<0.0001
Lo in SA
Hi in SA
Frequency (%)
Seed position

Figure 5

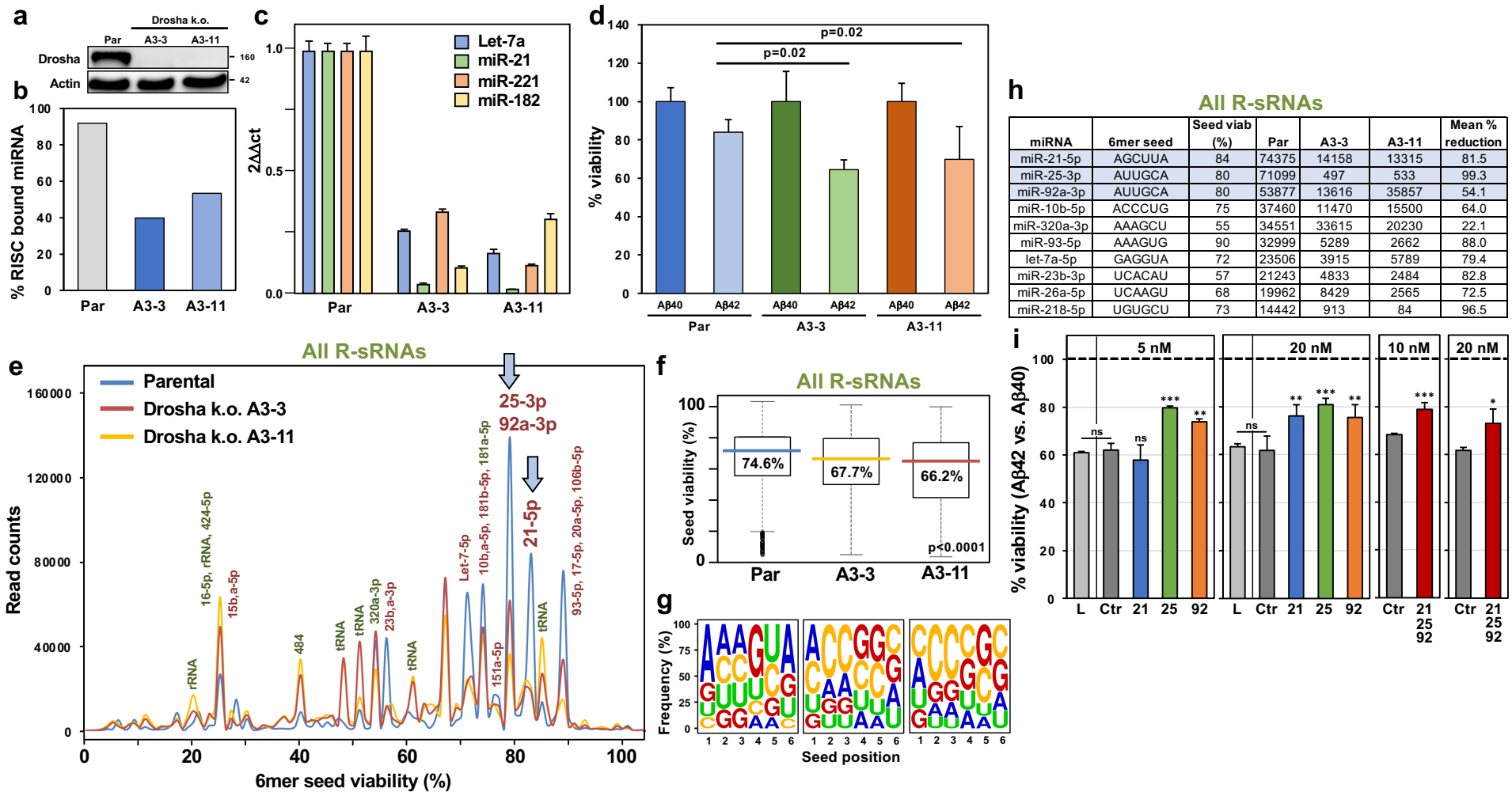

miRNA	6mer seed	Seed viab (%)	Par	A3-3	A3-11	Mean % reduction
miR-21-5p	AGCUUA	84	74375	14158	13315	81.5
miR-25-3p	AUUGCA	80	71099	497	533	99.3
miR-92a-3p	AUUGCA	80	53877	13616	35857	54.1
miR-10b-5p	ACCCUG	75	37460	11470	15500	64.0
miR-320a-3p	AAAGCU	55	34551	33615	20230	22.1
miR-93-5p	AAAGUG	90	32999	5289	2662	88.0
let-7a-5p	GAGGUA	72	23506	3915	5789	79.4
miR-23b-3p	UCACAU	57	21243	4833	2484	82.8
miR-26a-5p	UCAAGU	68	19962	8429	2565	72.5
miR-218-5p	UGUGCU	73	14442	913	84	96.5

Figure 6

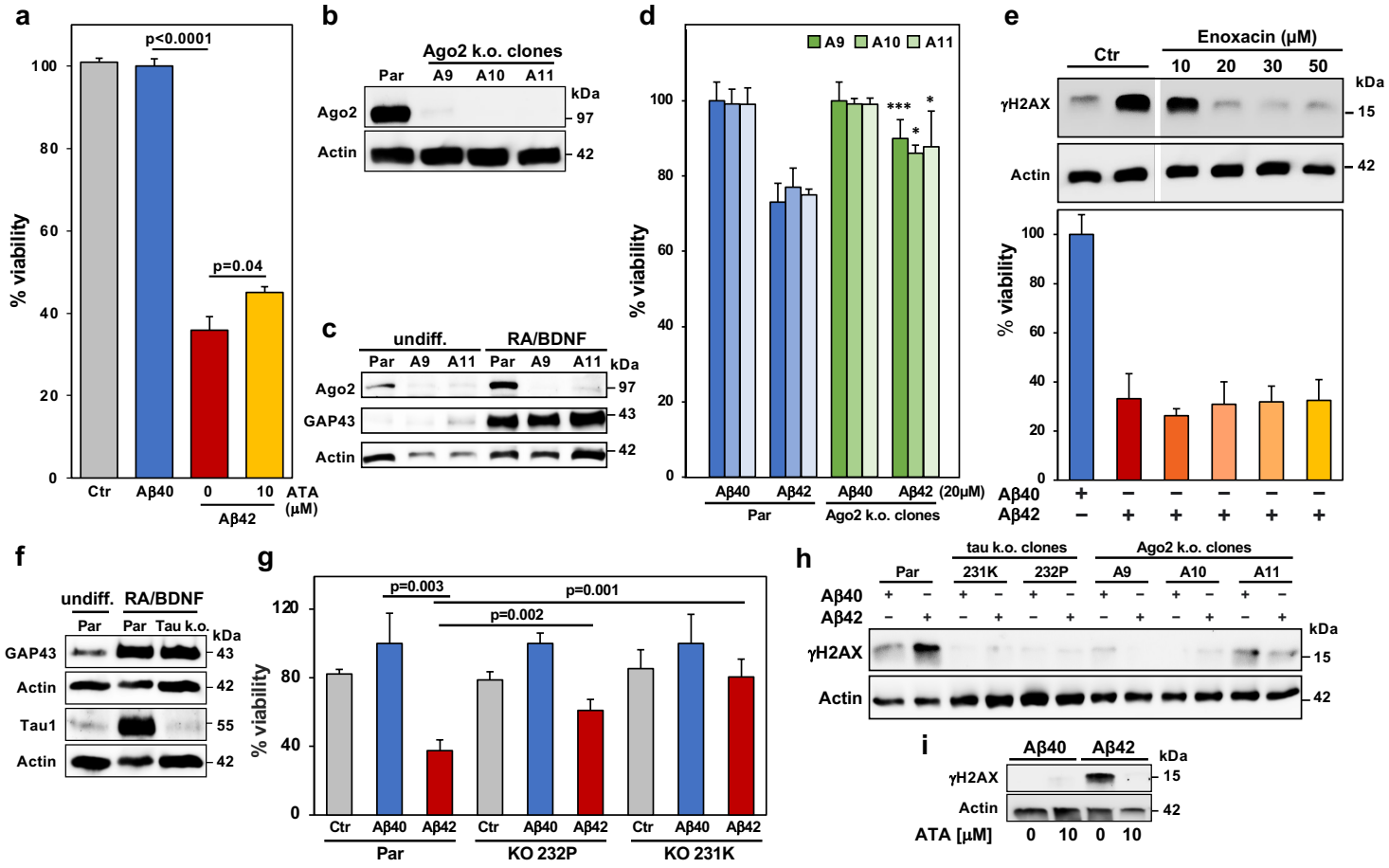
a
p<0.0001
p=0.04
% viability
Ctr
Aβ40
0
10
ATA (μM)
Aβ42
b
Ago2 k.o. clones
Par
A9
A10
A11
Ago2
Actin
kDa
97
42
c
undiff.
RA/BDNF
Par
A9
A11
Ago2
GAP43
Actin
43
d
A9
A10
A11
***
*
Aβ40
Aβ42
(20μM)
Par
Ago2 k.o. clones
e
Ctr
Enoxacin (μM)
10
20
30
50
γH2AX
Actin
15
42
f
undiff.
RA/BDNF
Par
Tau k.o.
GAP43
Actin
Tau1
55
g
p=0.003
p=0.001
p=0.002
Ctr
Aβ40
Aβ42
KO 232P
KO 231K
h
tau k.o. clones
Ago2 k.o. clones
231K
232P
i
ATA [μM]

Figure 7

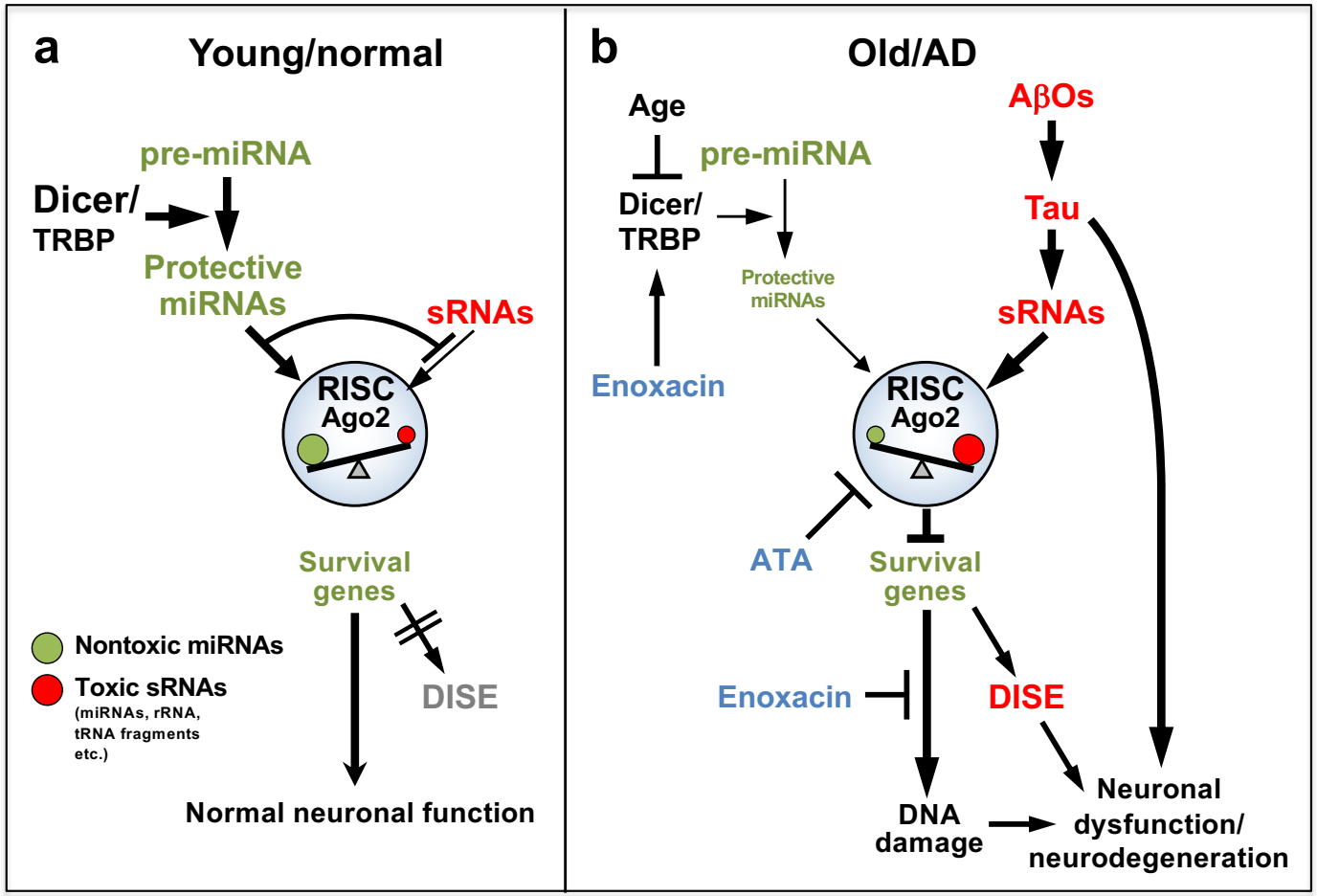
a
Young/normal
pre-miRNA
Dicer/
TRBP
Protective
miRNAs
sRNAs
RISC
Ago2
Survival
genes
DISE
Nontoxic miRNAs
Toxic sRNAs
(miRNAs, rRNA,
tRNA fragments
etc.)
Normal neuronal function
b
Old/AD
Age
pre-miRNA
Dicer/
TRBP
Protective
miRNAs
AβOs
Tau
sRNAs
Enoxacin
RISC
Ago2
ATA
Survival
genes
Enoxacin
DISE
DNA
damage
Neuronal
dysfunction/
neurodegeneration